ARL 72-0037
MARCH 1972

Aerospace Research Laboratories

TWO-PHASE VORTEX INVESTIGATION RELATED TO THE COLLOIDAL CORE NUCLEAR REACTOR

W. S. LEWELLEN

D. B. STICKLER

MASSACHUSETTS INSTITUTE OF TECHNOLOGY
CAMBRIDGE, MASSACHUSETTS

DDC
RECEIVED
19 JUN 1972
D

AIR FORCE SYSTEMS COMMAND
United States Air Force

NOTICES

When Government drawings, specifications, or other data are used for any purpose other than in connection with a definitely related Government procurement operation, the United States Government thereby incurs no responsibility nor any obligation whatsoever; and the fact that the Government may have formulated, furnished, or in any way supplied the said drawings, specifications, or other data, is not to be regarded by implication or otherwise as in any manner licensing the holder or any other person or corporation, or conveying any rights or permission to manufacture, use, or sell any patented invention that may in any way be related thereto.

Agencies of the Department of Defense, qualified contractors and other government agencies may obtain copies from the

Defense Documentation Center
Cameron Station
Alexandria, Virginia 22314

This document has been released to the

CLEARINGHOUSE
U. S. Department of Commerce
Springfield, Virginia 22151

for sale to the public.

Copies of ARL Technical Documentary Reports should not be returned to Aerospace Research Laboratories unless return is required by security considerations, contractual obligations or notices on a specified document.

DOCUMENT CONTROL DATA - R & D

(Security classification of title, body of abstract and indexing annotation must be entered when the overall report is classified)

1 ORIGINATING ACTIVITY (Corporate author)	2a. REPORT SECURITY CLASSIFICATION
Massachusetts Institute of Technology Cambridge, Massachusetts 02139	UNCLASSIFIED
	2b GROUP

3 REPORT TITLE

Two-Phase Vortex Investigation Related to the Colloidal Core Nuclear Reactor

4 DESCRIPTIVE NOTES (Type of report and inclusive dates)
Scientific, Final   15 Sept 70 - 9 Dec 71

5 AUTHOR(S) (First name, middle initial, last name)

W. S. Lewellen and D. B. Stickler

6 REPORT DATE	7a. TOTAL NO. OF PAGES	7b. NO. OF REFS
March 1972	47	17
8a. CONTRACT OR GRANT NO F33615-71-C-1045	9a. ORIGINATOR'S REPORT NUMBER(S)
b. PROJECT NO 7116	
c. DOD Element 61102F	9b. OTHER REPORT NO(S) (Any other numbers that may be assigned this report)
d. DOD Subelement 681308	ARL 72-0037

10 DISTRIBUTION STATEMENT

Approved for public release; distribution unlimited

11 SUPPLEMENTARY NOTES	12 SPONSORING MILITARY ACTIVITY
TECH OTHER	Aerospace Research Laboratories Energy Conversion Research Lab (LE) Wright-Patterson AFB, Ohio 45433

13 ABSTRACT

Liquid containment in a gas-driven vortex has been investigated both experimentally and theoretically. Average air-water mixture densities greater than 100 times the thru-flow gas density were contained in a vortex chamber while maintaining the loss rate of water at that due to vaporization. Interaction studies indicate a stronger coupling of the liquid to the gas than of the liquid to the wall. Results are discussed in terms of their applicability toward estimating the potential performance of a colloidal core nuclear reactor.

DD FORM 1473 (1 NOV 65)

III

14 KEY WORDS	LINK A		LINK B		LINK C	
	ROLE	WT	ROLE	WT	ROLE	WT
Two-Phase Vortex						
Liquid Particle Containment						
Cylindrical Wall Boundary Layer						
Colloid Core Nuclear Reactor						
Vortex Chamber						
Heat Transfer						

IV

ARL 72-0037

TWO-PHASE VORTEX INVESTIGATION RELATED TO THE COLLOIDAL CORE NUCLEAR REACTOR

W. S. LEWELLEN

D. B. STICKLER

MASSACHUSETTS INSTITUTE OF TECHNOLOGY

CAMBRIDGE, MASSACHUSETTS

MARCH 1972

FOREWORD

This report is a final report on research carried out at the MIT Space Propulsion Laboratory under Contract F 33615-71-C-1045 during the period September 15, 1970 to December 9, 1971. The major results of this study have been included in a paper published in the Proceedings of the 2nd Symposium on Uranium Plasmas: Research and Applications held at Atlanta, Georgia on November 15-17, 1971. Contributions to this research have been made by Prof. C. K. W. Tam, Prof. J. L. Kerrebrock, Mr. P. J. Cox, Mr. P. W. Jones and Mr. H. L. Kantha. The work is being continued under Contract F 33615-72-C-1344.

LIST OF ILLUSTRATIONS

VI

LIST OF ILLUSTRATIONS CON'T

1. INTRODUCTION

The attractiveness of energy obtained from controlled nuclear fission would be enhanced for both space and earth-based operation if a practical means of increasing the fuel operating temperature could be engineered. Numerous conceptual engineering approaches to this goal have been proposed in the past several years. Recent work[1] includes several schemes, including gaseous, particulate, and liquid phase nuclear fuel, with both radiative and conductive-convective heat transfer to a working fluid considered. In the work here reported, a two phase flow scheme utilizing vortex containment of condensed phase nuclear fuel is investigated. This work is both comparable and complementary to work carried out in-house at ARL [2,3,4] on the use of solid particulate nuclear fuel contained in a hydrogen vortex. However, the liquid fueled system has a higher potential specific impulse than does the solid particle case. Also, it is not subject to a potential local melt-down or caking instability which the particle fuel system could exhibit. We assume the use of a molten uranium carbide-zirconium carbide fuel, with a hydrogen working fluid injected into the reactor, and exhausting through a nozzle on the longitudinal axis of the system. A complex fluid dynamic and transport process situation is to be expected. Heat transfer from fuel to wall and from fuel to working fluid, as well as fuel mass transport out the nozzle, are of clear import to the potential performance of this system, and are dependent upon the fluid flow field established.

Two of the basic problems which must be solved in investigating the feasibility of any advanced reactor concept are those associated with adequate fuel containment and sufficient energy transfer from the fuel to the working fluid. Of course, these are in turn strongly coupled to questions of neutronic behavior, material restrictions, control systems, operational economics, social acceptance, etc. In this paper we primarily confine our attention to the questions of containment and energy transfer. The basic question we consider is how much liquid may be contained in a cylinder in such a manner that energy may be transferred from the liquid to a gas flowing thru the cylinder without too large a fraction of the energy flowing thru the cylindrical walls. Our preliminary answer to this question is then discussed in terms of its applicability toward determining the feasibility of a reactor concept.

Vortex flow has long been used as a means of separating fine particles and small droplets from a gas and a great deal of literature surrounds the subject[5]. With a few notable exceptions[3,4] past investigators have dealt with flows with relatively low particle loadings since they were interested in efficient separation rather than containment. For neutronic criticality to be achieved by containing fuel alloys with relatively low volatility in a small reactor, it is necessary for the mass ratio of contained material to contained gas to be large, of the order of 10^2[6]. Such ratios have been achieved with dust in air in certain geometries[3,4]. The next section describes a small model experiment which demonstrates that such mass ratios of liquid-to-gas may be obtained in a relatively unrestricted geometry. Section 3 describes results of the variation in containment limits with certain geometrical and fluid properties.

Containing the fuel is only part of the problem. The operating temperature of the fuel is a function of the allowable wall temperature as long as a fraction of

the energy from the fuel is transferred to the gas via the wall. Thus a significant fraction of the energy must be transferred directly from the fuel to the working gas. A simple energy balance shows that if the final gas enthalpy is to be 2 times that at the wall temperature (a rough upper bound on what might be expected from a liquid core reactor due to fuel vaporization limits on fuel temperature) then the energy transferred directly to the gas from the fuel must be equal to that transferred via the wall. Thus the interaction between the contained fuel and gas should be equal to or larger than the interaction between the fuel and the wall. Section 4 describes the results of experiments designed to estimate such interactions in the model geometry under various conditions.

Section 5 is involved with theoretical aspects of two-phase flow in a vortex. It provides a simple estimate of containment limits as a function of geometry and fluid properties. A model of the two phase flow field near the wall for the solid particle-gas system is proposed and analyzed in Appendix B. The predicted wall shear behavior is employed in Section 5.

2. DESCRIPTION OF EXPERIMENTAL MODEL

A schematic of the experimental model is shown in Fig. 1. We chose a length-to-diameter ratio equal to 1 for the cylindrical vortex chamber as neutronically most favorable. For other things equal this should minimize the fuel required for criticality since it minimizes the surface area for a given volume. We wanted the swirl angle of the gas flow thru the chamber to be one of the major variables. We also wanted the entering flow to be as uniformly distributed over the wall as possible to help in minimizing the interaction between the internal flow and the wall.
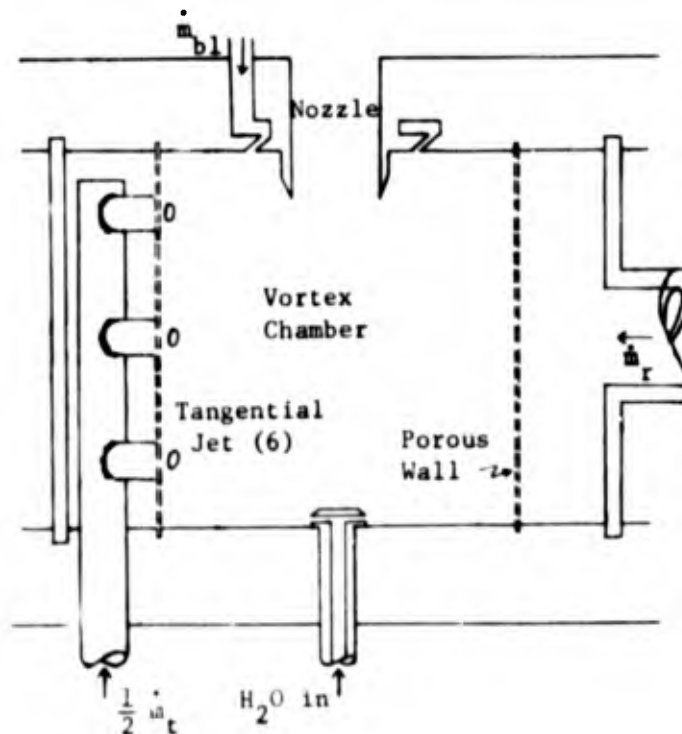
Fig. 1 Schematic of Experimental Vortex Chamber

2

Ideally this could be achieved by varying the angle of a very large number of small holes evenly distributed over the wall. As a compromise we used a porous cylinder with 6 tangential injection jets and designed the flow system for independent control between the radial flow thru the porous cylinder and the tangential flow. A 4 inch diameter cylinder was a convenient size with which to work for the available laboratory compressor air system. An internal view of the model is given in Fig. 2.
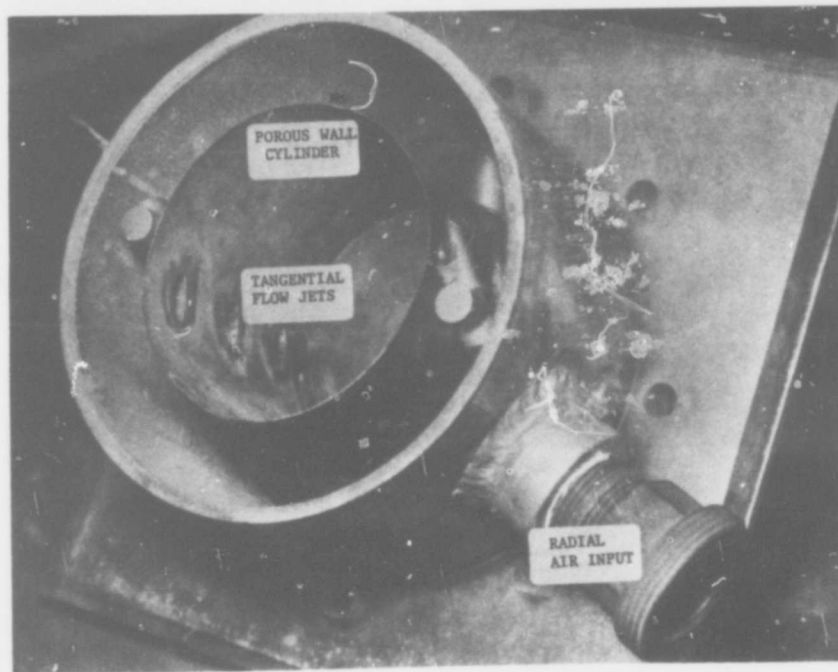
Fig. 2   Internal View of Porous Cylinder and Radial Plenum

Two features were incorporated in the neighborhood of the exhaust hole to enhance the containment of very small droplets. The geometry of this exhaust region is shown in Fig. 3. Cyclone separators have long used a so-called "vortex finder" to improve the efficiency of separation by preventing the boundary layer on the exhaust end wall from carrying the particles directly into the exhaust[7]. This "vortex finder" is a thin cylindrical sleeve extended about 1 exhaust radius into the chamber. This forces any flow escaping directly from the end wall boundary layer into the exhaust to negotiate a very sharp turn which aids in separating out any particles in that flow. Extensive studies at the Aeronautical Research Laboratory[3] have shown that injection of flow with a high angular momentum directly into the end wall boundary layer can also be quite effective in preventing flow from passing directly from the boundary layer into the exhaust. We included an independently controlled boundary-layer-control (BLC) flow thru four 1/16 inch diameter holes evenly spaced around the perimeter of a circle about 1/4 inch outside the exhaust radius. The holes met the plexiglass surface at a 20° angle in such a way that the major velocity component of air leaving the holes was tangential. The BLC flow was introduced with the same swirl direction as the primary tangential flow.

3
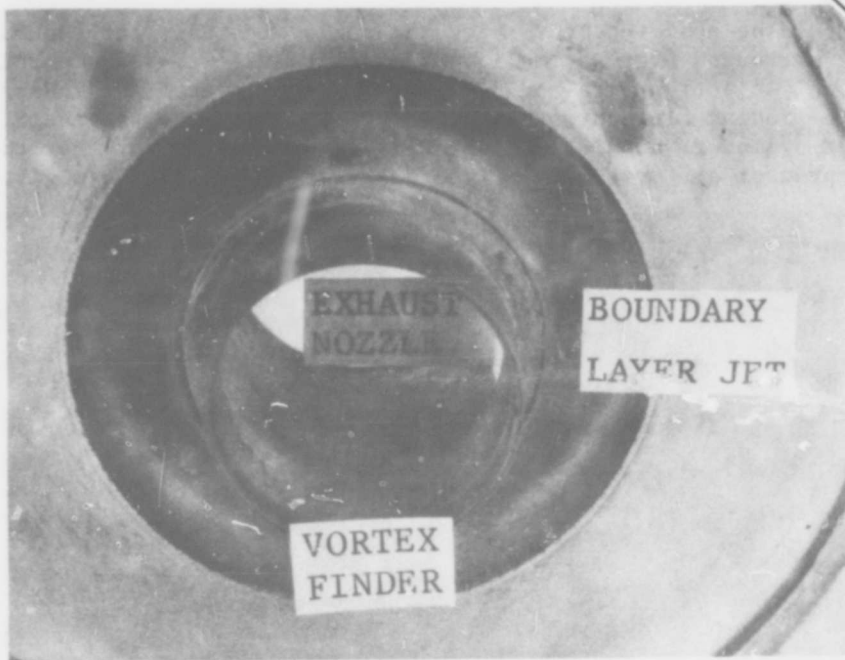
Fig. 3 Close-up View of the Exhaust Region

Air was supplied to the model from a 60 psig pressure compressor thru an alum-
ina pebble bed dehumidifier. Suitable valving permitted the flow to be divided
into 4 branches leading respectively to the radial flow thru the porous cylinder,
the main tangential flow, the boundary-layer-control flow, and a cross flow intro-
duced downstream of the vortex chamber which permitted some control of the exhaust
pressure and the exhaust gas humidity. Each of the 4 branches could be independ-
ently controlled and their flow rates measured.

The exhaust from the vortex chamber was connected to a steam ejection vacuum
system (minimum pressure 2 psia) thru a pyrex glass cross which can be clearly seen
in the overall view given in Fig. 4. The vortex chamber is connected to the bottom
arm of the cross, the right arm is connected to the exhaust system, the previously
mentioned cross flow is fed into the left arm, and the top is covered with plexi-
glass to make it possible to look down into the vortex chamber. Both end walls of
the vortex chamber are plexiglass with the exhaust hole in the top end wall.

Measured amounts of liquid could be introduced into the vortex chamber thru a
hollow screw in the bottom plexiglass plate. The top of the screw was raised
slightly above the inner surface of the plate to permit radial injection of the
liquid thru 3 holes in the screw at a flow rate suitable for adequate momentum
transfer from the gas vortex to the liquid.

We used two different exhaust plates, one with a 1 inch diameter exhaust hole,
and the other with a 1/2 inch diameter exhaust; and three different porosities in
the porous cylinder. The basic cylinder used for most of the results was 0.0245
inches thick with uniformly distributed holes of 0.005 inch diameter for a 1% open

4
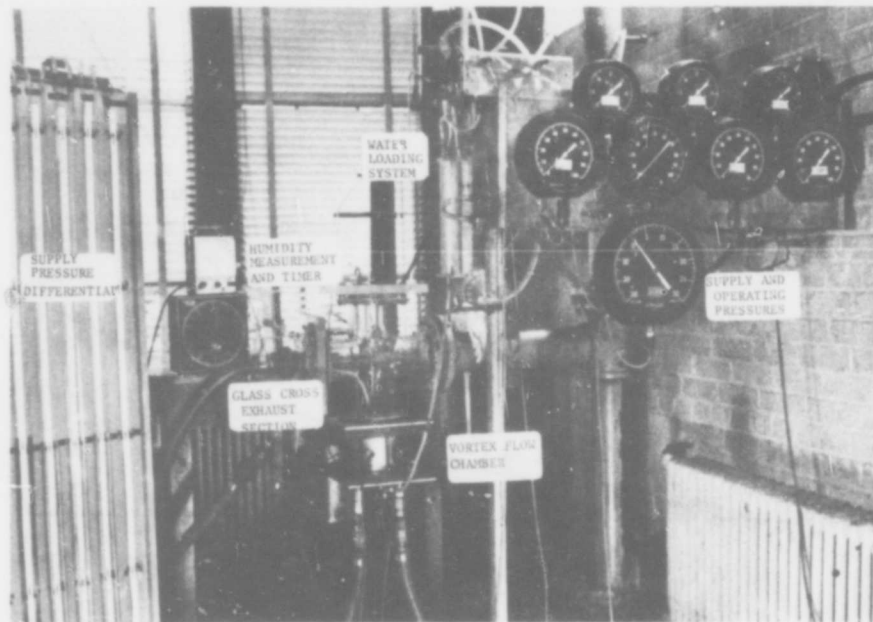
Fig. 4   Overall View of Experimental Apparatus

area. This open area for the radial flow was reduced by a welding seam and by the
tangential jets and the soldered area around them to 0.5% for one cylinder and to
0.7% for another. It was further reduced to 0.3% by partial taping of the holes
for other tests. The pressure drop characteristic of each of these cylinders is
given as a function of radial mass flow in Fig. 5. Flow was in each case single
phase, and vortex chamber pressure was slightly in excess of one atmosphere abso-
lute.

3.   LIQUID CONTAINMENT LIMITS

There are three mechanisms by which the liquid can be lost from the chamber:
1) it may vaporize and escape with the gas, 2) small droplets may be entrained into
the exhaust gas, or 3) an instability can cause the liquid to leak radially outward
thru the porous cylinder. The vapor losses are primarily determined by the vapor
pressure of the liquid and the extent of the interaction between the liquid and
gas. This section deals with the last two mechanisms. Small droplets may be ex-
pected to be lost when there is not a sufficient swirl angle in the exhaust flow to
separate out the droplets as the gas exhausts. On the other hand, when the swirl
angle is large and the radial flow thru the porous cylinder is continually de-
creased, a point is reached where the pressure drop across the porous cylinder is
not adequate to stabilize the liquid-gas interface against centrifugal instabili-
ties and the liquid is forced radially outward thru the porous cylinder.

Figure 6 shows the containment limits for 3 different fixed tangential flows.
The left hand side of the containment envelope marks the flow ratio at which
increased radial flow makes water droplets detectable in the exhaust flow. Two

5
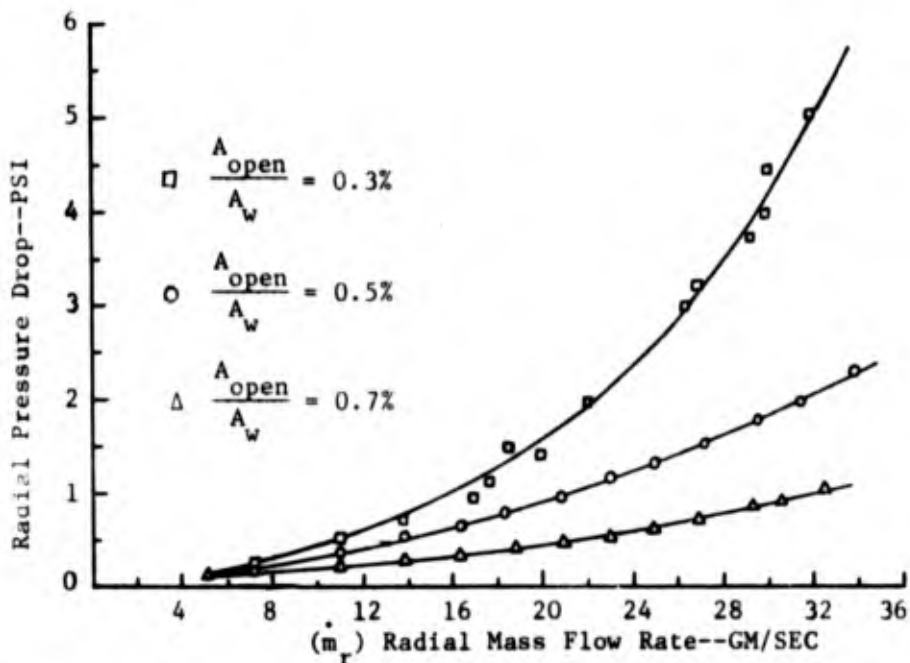
Fig. 5 Radial Pressure Drop Across the Porous Cylinder as a Function of
the Radial Mass Flow Rate and Cylinder Porosity

methods were used to detect droplets in the exhaust, a moisture sensitive element placed in the glass cross near the chamber exhaust and direct visual inspection of the exhaust flow. As the containment envelope is crossed, small increases in radial flow produce large increases in droplet spray out the exhaust. Thus the visual spray point appeared to be a reliable means of determining the left-hand boundary of the containment curve. The right-hand side of the containment curve was obtained by electrically monitoring the plenum outside the porous cylinder. When a small amount of water leaked thru the porous cylinder to the bottom of the plenum it registered as a voltage change in a circuit designed for this purpose. The largest source of error in Fig. 6 is related to knowing exactly how much water is contained in the cylinder. A measured amount of water was introduced into the chamber with the radial flow set at a value which insured containment, then the radial flow was increased or decreased to approach the left or right containment boundary. Since this operation required several seconds some water was always lost by vaporization before the containment boundary was reached. The containment points on the left boundary are probably subject to a 10% error for this reason. As the tangential flow is increased the containment envelope shifts down and to the right. The increase in inertial forces apparently breaks the water into smaller droplets which require stronger swirl in the exhaust for separation.

The effect of different values of exhaust hole area and boundary-layer-control flow on the containment envelope is shown in Fig. 7. More water can be contained in the chamber with the smaller exhaust hole. Also it can be seen that adding the BLC flow greatly expands the containment region. It is possible that larger values of BLC flow would further increase containment. No tests have yet been made at

6

larger values. At the peak values of ρ_{av} in Fig. 7, water occupies roughly 20% of the volume of the chamber.
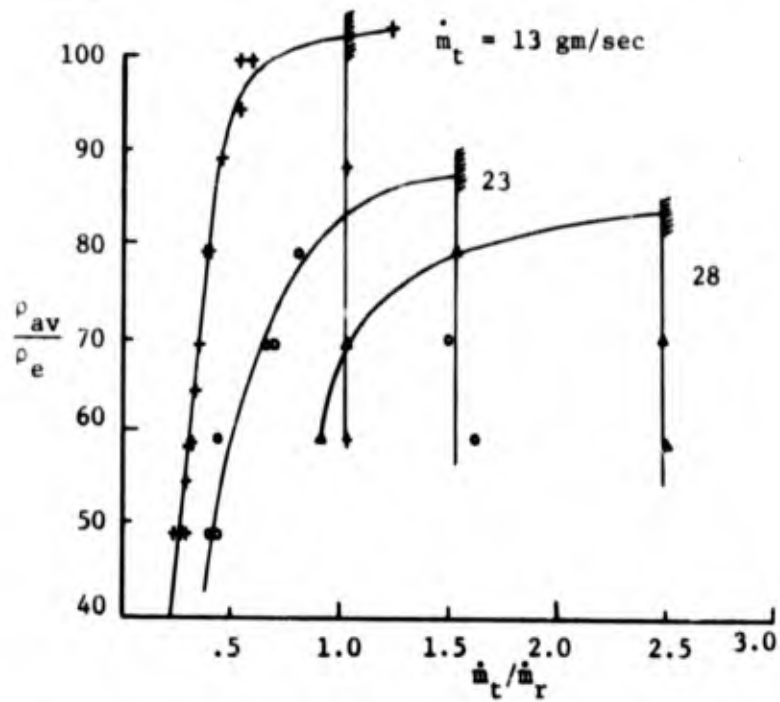
Fig. 6 Envelope of maximum water containment as a function of tangential-to-radial mass flow ratio for $r_e/r_o = 1/4$, $\dot{m}_{b.1.} = 4.2$ gram/sec and 3 values of $\dot{m}_t$.
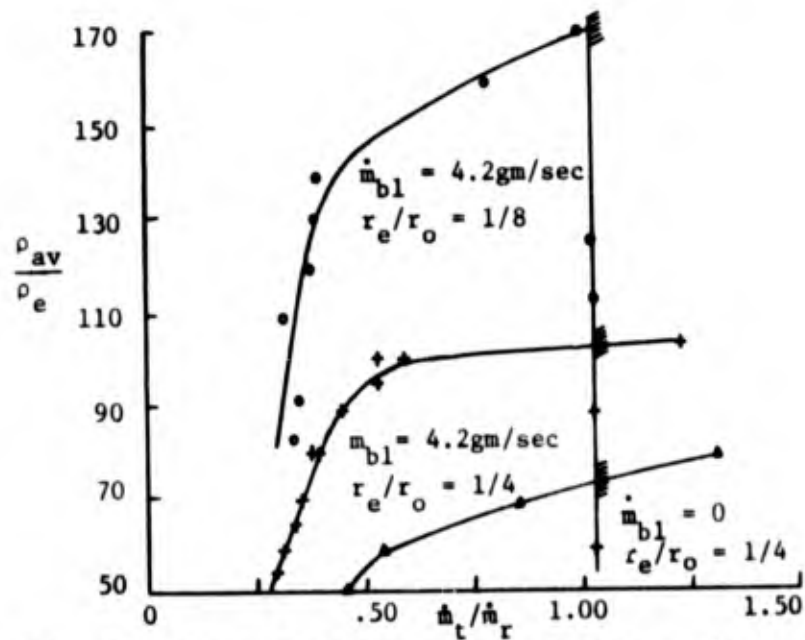
Fig. 7 Envelope of maximum water containment for different values of r_e/r_o and $\dot{m}_{b.1.}$ for $\dot{m}_t = 13$ gram/sec

7

Figure 8a and b are photographs of the vortex chamber as viewed from above. Figure 8a is a view of the empty chamber. The gray outer annular region is the interior of the porous cylinder. The rings near the center are the BLC jets and the "vortex finder". The unfocused region in the center is the water injection device on the bottom plate. The tube and fitting attached to the top plate is the BLC feed pipe. Figure 8b is the same view of the chamber while it is in operation with approximately 100 milliliters of water (over 10% of the chamber volume). The water appears to be confined largely to an outer annular region of approximately 1/2 of the chamber volume. The ripples on the under surface of the top plate indicate the spirals visible in the end wall boundary layer. Water continually spirals inward thru the 2 end wall boundary layers but little of this appears to be lost out the exhaust. Instead, it is centrifugally separated out from the exhaust gas and returned thru the main part of the chamber to the outer annulus of liquid.

a) no water
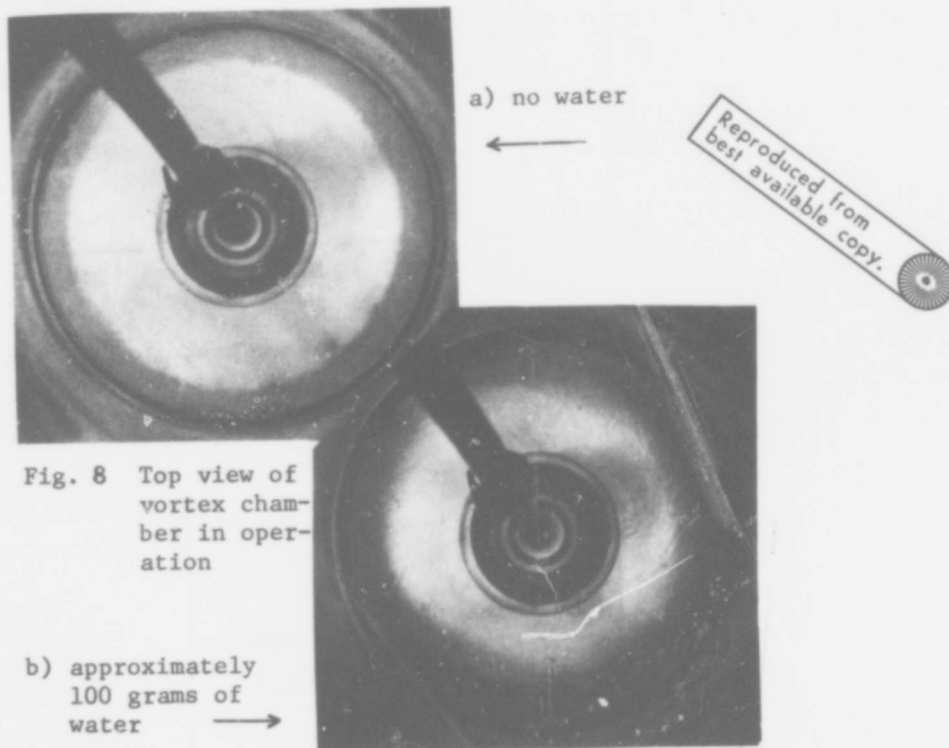
Fig. 8 Top view of vortex chamber in operation

b) approximately 100 grams of water

Figure 9 gives a clue to what happens within the chamber as the liquid loading is increased. The radial pressure gradient is balanced by the product of the density and the centrifugal force, i.e.

$$\Delta p = \int_o^{r_o} \frac{\rho v^2}{r} \, dr \tag{1}$$

In order for Δp to decrease as ρ increases it is necessary to have a sharp drop in v. The drop in v is brought about by a loss in recovery factor, v_o/v_t, as the wall shear increases with increasing density. As loading is continually increased v is decreased until a point is reached where the water droplets can no longer be contained and water sprays out of the chamber.

8
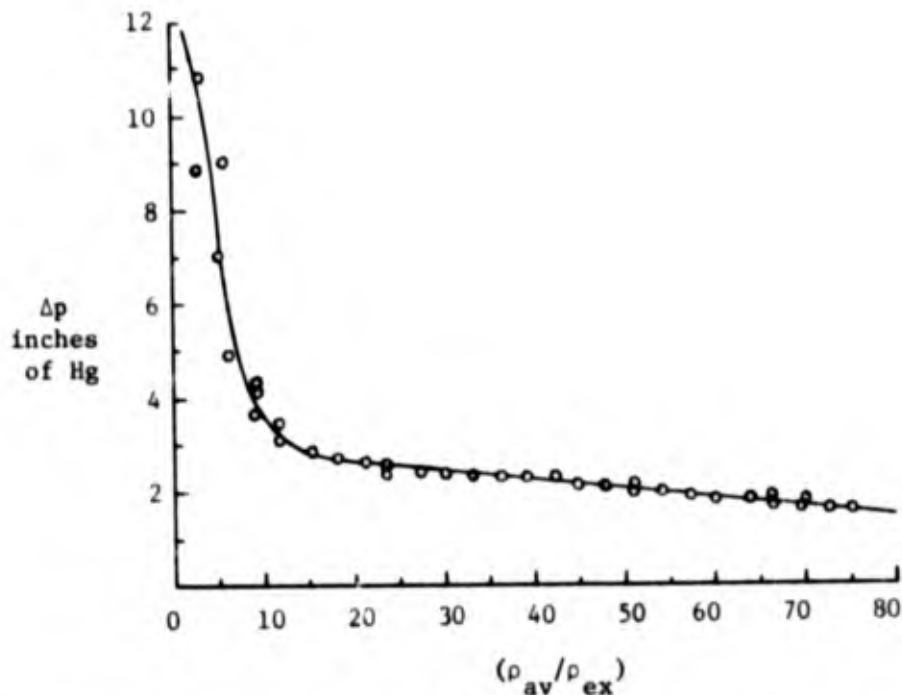
Fig. 9 Pressure Drop Across the Vortex as a Function of the Chamber Density for r_o/r_e = 4, $\dot{m}_t/\dot{m}_r$ = 0.7 and $\dot{m}_t$ = 13 gram/sec

The influence of changing the porosity of the cylinder is shown in Fig. 10. There is no discernible effect on the spray point, the left-hand side of the containment envelope. The right-hand side of the envelope shifts right as the porosity of the cylinder is decreased to increase the pressure drop across the cylinder (See Fig. 5). Note that the three points for the 0.7 percent porosity data which do not lie near the curve are suspect. These points have not been checked because of the destruction of the copper cylinder in a wall interaction test.

Figure 11 shows the effect on containment of a one third reduction in the total tangential injection area. The nominal tangential jets are .25 inch in diameter – giving a total injection area of .3 in^2 for the six jets. Employing drilled and tapped plugs, the total area is reduced to .2 in^2. The effect of the area reduction on containment is very similar to the effect of a tangential mass flow increment, as seen in Figure 6. The data in Figure 11 represents lines of constant tangential mass flow rate. From continuity, the tangential velocities are computed to be 175 ft/sec and 272 ft/sec for the total tangential-to-exhaust area ratios ($6d^2_{tan}/d^2_{ex}$) of .38 and .24 respectively.

A dependence of the spray point on liquid surface tension is shown in Fig. 12. A decrease in surface tension by adding Dupont "Zonyl A" to the water produced a marked reduction in the containment envelope. This is consistent with the expectation that the water droplet sizes near the center of the chamber should depend on surface tension, σ, decreasing in size as σ decreases. Thus stronger swirl should be required to contain the same amount of liquid when σ is reduced.

9
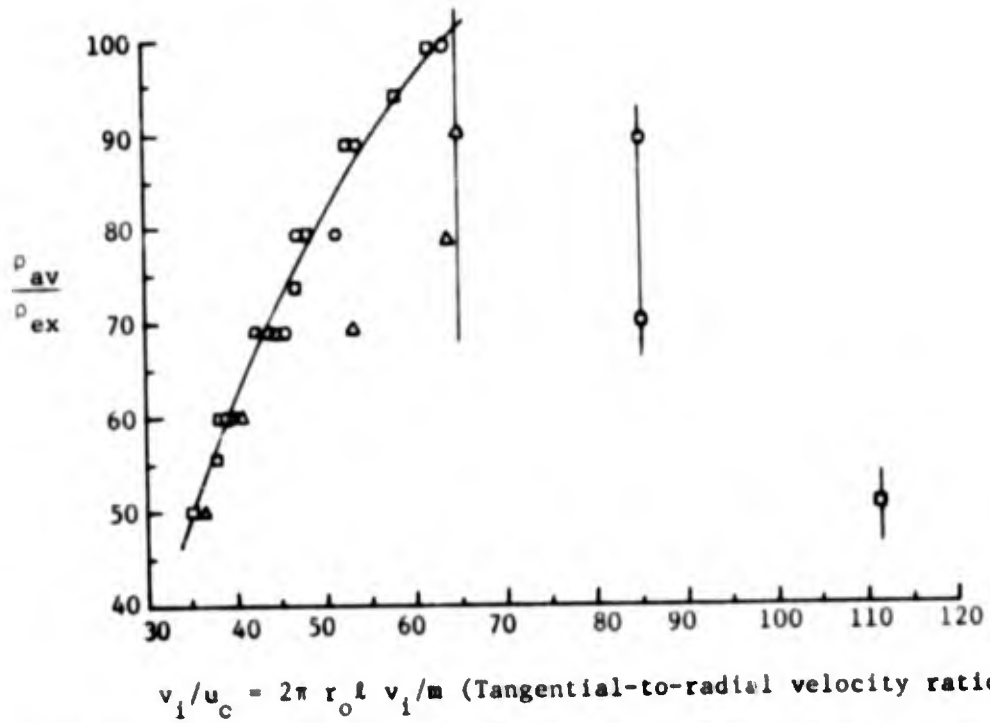
Fig. 10 The influence of radial flow open area (cylinder's porosity) on fluid containment. ($\square$ – 0.3%, $\circ$ – 0.5% and $\triangle$ – 0.7% porosity)
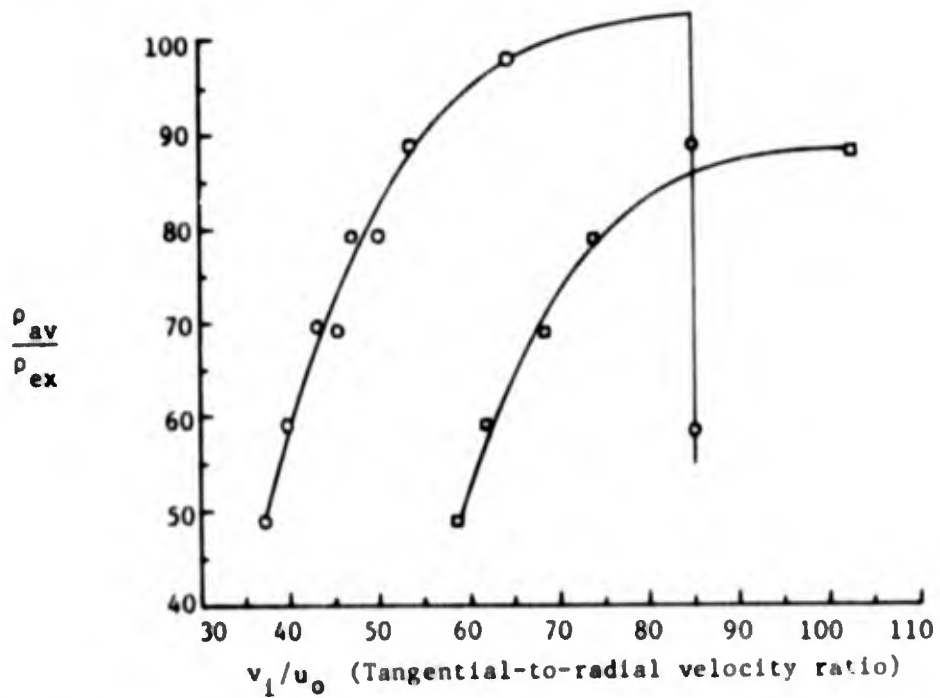
Fig. 11 Influence of tangential injection area on containment with constant tangential mass flow rate of 12.5 gm/sec. ($\circ$ – A_t/A_{ex} = 0.38, $\square$ – A_t/A_{ex} = 0.24)

Within the containment envelope, liquid losses appeared to be limited to vaporization losses. This was checked by measuring the humidity in the exhaust and by measuring the time required for the liquid to slowly disappear from the chamber. The air-to-water mass flow ratios obtained by these two methods are shown in Figs. 13 and 14. The estimates in Fig. 13 were obtained using a wet bulb and a dry bulb thermometer placed far downstream of the chamber exhaust. The estimates in Fig. 14 were obtained by measuring the time required to empty a given water loading from the chamber and calculating a time-averaged loss rate. Neither method was considered satisfactory for precise measurements and thus the trends exhibited in Figs. 13 and 14 as a function of ρ_{av}/ρ_{ex} and v_1/u_o are probably not reliable. However, both methods indicate that the exhaust air is near saturation conditions.
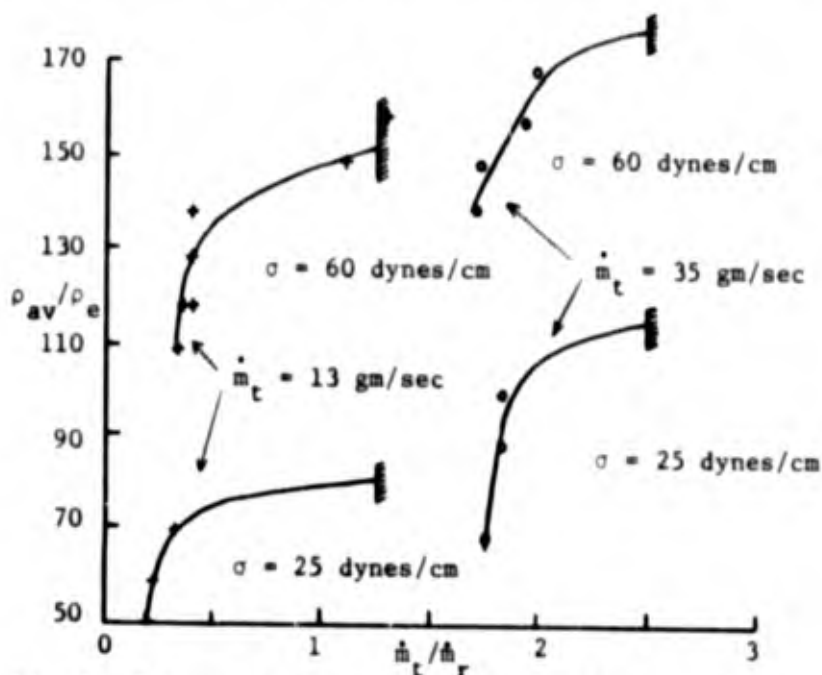
Fig. 12 Exhaust spray envelope for different values of surface tension ($r_e/r_o = 1/4$, $\dot{m}_{b.1.} = 4.2$ gram/sec)

4. ESTIMATES OF LIQUID INTERACTION

In order for our experimental chamber to be an attractive model for a reactor concept it is necessary to have the liquid strongly coupled to the gas with relatively weaker coupling to the wall. In measuring a liquid-gas interaction, it was assumed that heat transport in the gas phase represented the dominant resistance. With this assumption, a mass transport analogue was employed. The interaction was measured by monitoring the reaction between HCl added to the air and AgNO$_3$ added to the water. The kinetic rate of the reaction between these two reactants is sufficiently rapid that all of the HCl diffusing to the liquid should react to form AgCl. Measuring the difference between entering and exiting concentrations of HCl in the gas then provides a direct measure of the mass transfer between gas and liquid. This may be written as

$$\int_{\substack{gas-liquid \\ interface}} C_s \, x \, dA = \dot{m} \, (x_1 - x_e)$$

(2)

11
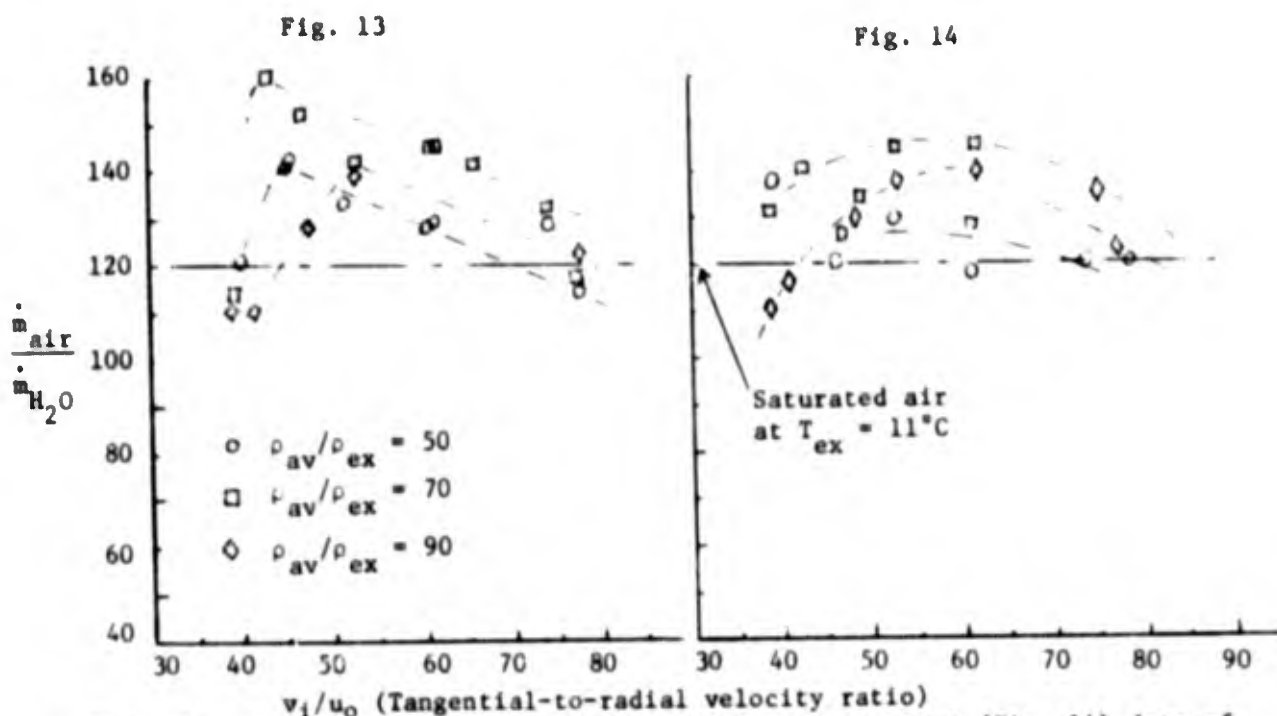
Figs. 13 and 14 Psychrometric (Fig. 13) and time averaged (Fig. 14) data of the air-to-water mass flow rate for $r_o/r_e = 4$ and $\dot{m}_t = 13$ gm/sec

with C_s a mass transfer coefficient between gas and liquid, and x the concentration of the reactive species in the gas. A similar equation can be written for heat transfer

$$\int_{\substack{\text{gas-liquid} \\ \text{interface}}} C_h (T_\ell - T_g) \, dA = \dot{m} \, C_p \, (T_e - T_w) \tag{3}$$

If the liquid temperature were assumed constant, then these equations would be similar and assuming similarity between heat and mass diffusion (i.e. assuming Lewis number = 1) would give

$$\frac{T_\ell - T_e}{T_\ell - T_w} = \frac{x_e}{x_i} \tag{4}$$

In a reactor, T_ℓ would not be constant, increasing with decreasing radius, so Eq. (4) cannot be applied directly. If T_ℓ is interpreted as the peak liquid fuel temperature, a somewhat optimistic estimate for T_e results. However, the above discussion does show that the concentration ratio provides a quantitative measure of the liquid-gas interaction.

Figure 15 is a plot of the concentration ratio as a function of mass flow ratio with 70 grams liquid in the chamber. There is considerable scatter to the data due to the difficulty of accurately determining x_i and x_e[8], but the indication of a strong interaction between the liquid and gas is evident even in the

12

lowest recorded value of $x_i/x_e \cong 20$.
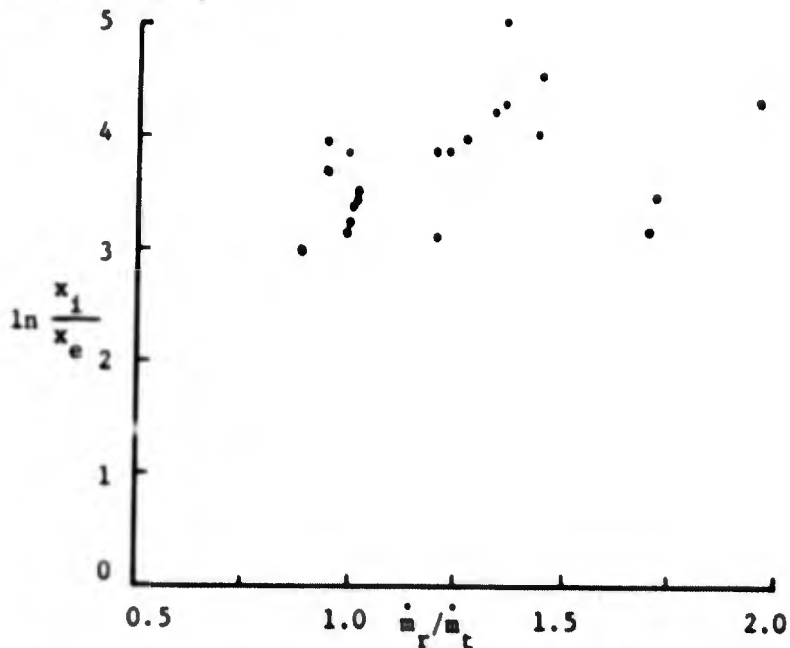
Fig. 15 Gas-liquid interaction as estimated from
the change in gas reactant concentrations
($\dot{m}_t = 13$ gram/sec, $\dot{m}_r = 4.2$ gram/sec,
$r_e/r_o = 1/4$, and $\rho_{av}/\rho_e = 70$)

We tried to use the same chemical analogy to heat transfer to quantify the
liquid-wall interaction[8]. We used a copper wall and a nitric acid solution, but
the reaction proved to be kinetically controlled, rather than controlled by mass
transport as desired. We were unable to satisfactorily interpret the results as a
quantitative measure of the liquid-wall interaction. See Appendix A for further
details.

An estimate of the liquid-wall interaction was obtained by estimating wall
shear. By using an angular momentum balance to relate skin friction to jet veloc-
ity recovery factor and Reynold's analogy to relate skin friction to heat transfer
film coefficient, an expression from the next section Eq (25) may be used as a
measure of the liquid wall interaction, S, defined as

$$S = \frac{h_o}{h_w} - 1 = \dot{m} \left(\frac{C_p}{C_h A}\right)_w \tag{5}$$

The parameters ρ_i, v_i, $\dot{m}_r$ and $\dot{m}_t$ in Eq (25) may be directly estimated from measure-
ments. The velocity v_o may be related to the pressure drop across the chamber by
using the radial momentum equation, Eq (1). If the liquid is assumed to be homo-
geneously mixed in an annulus between $\bar{r}$ and r_o and vr is constant in this region,
then Eq (1) may be integrated to give

$$v_o = \left[\frac{2\Delta p/\rho_o}{(r_o/\bar{r})^2 - 1}\right]^{1/2} \tag{6}$$

13

Also

$$\rho_o = \rho_{av}/[1 - (\bar{r}/r_o)^2] \tag{7}$$

so that

$$v_o = \left[\frac{2\Delta p}{\rho_{av}}\right]^{1/2} \frac{\bar{r}}{r_o} \tag{8}$$

From Fig. 8, $\bar{r}/r_o$ appears to be roughly 0.7. Using this value, Eq (5), Eq (7), and Eq (8) were used to estimate S along the containment line for $v_i = 180$ ft/sec. given in Fig. 6 and 7. The estimated values are given in Fig. 16 as a function of ρ_{av}/ρ_e. Considerable uncertainty is associated with these estimates, particularly because of the difference of two terms appearing in the denominator of Eq (25). Nevertheless it does show that values of S greater than one can be obtained along the containment curve. (Note that the liquid-wall interaction decreases with increasing S).
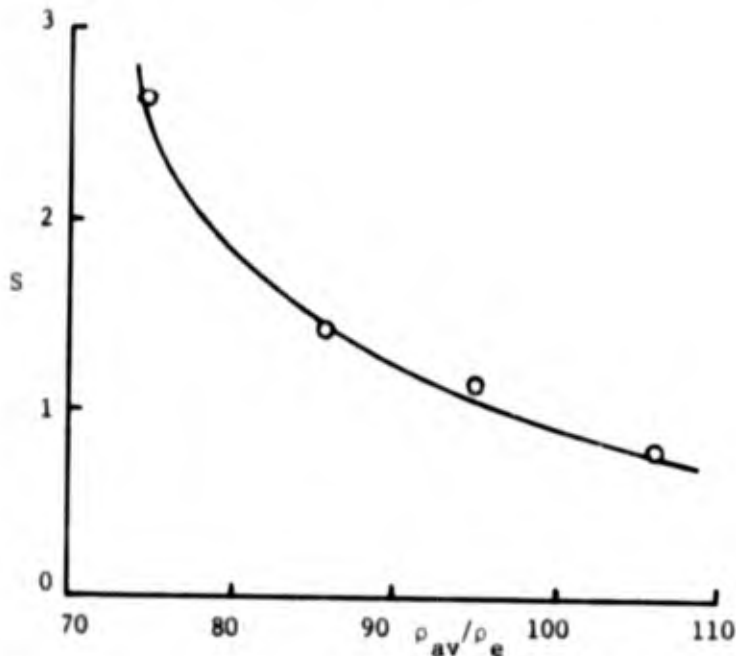
Fig. 16 Liquid-wall interaction, S, as estimated
from wall shear losses as a function of
ρ_{av}/ρ_e for operating conditions along the
top containment envelope of Fig. 6

Experiments are presently underway to more accurately determine the liquid-wall interaction by using direct heat transfer measurements.

If the liquid-gas interaction is interpreted as the product of a film coefficient and an interface area, then

$$(C_h A)_{l-g} = \dot{m} C_p \ln (x_i/x_e) \tag{9}$$

14

and this may be compared directly to the liquid-wall interaction.

$$\frac{(C_h A)_{\ell-g}}{(C_h A)_w} = S \ \ln \ (x_1/x_e) \tag{10}$$

Values of this ratio of liquid-gas conductance to liquid-wall conductance range from 2 to 15 for the conditions of Fig. 14. Although definitive conclusions must await more direct and accurate measurements, it does seem quite reasonable to expect that sufficiently low heat transfer to the wall could be maintained.

5. THEORETICAL ASPECTS OF TWO-PHASE FLOW IN A VORTEX

Particles should be essentially contained within a vortex chamber whenever

$$\frac{\pi}{9} \ (\frac{\rho_s}{\rho} - 1) \ \frac{\ell \ v_e^2 \ r_p^2}{\mu \ \dot{m}} \geq 1 \tag{11}$$

This criterion may be derived by assuming that the particle motion is governed by a balance between centrifugal force and Stoke's drag on the particle. The major qualification to this criterion is that particle losses thru the boundary layer on the wall surrounding the exhaust must not be permitted. Essentially the same result is obtained whether the radial thru flow is assumed to be uniformly distributed across the chamber or confined to the boundary layer opposite the exhaust[5].

The crucial questions involved in estimating the limits of containment are those concerned with estimating r_p and v_e. Let us first consider the case of solid particles with r_p given and try to estimate v_e from an angular momentum balance within the chamber. Angular momentum is introduced into the chamber thru the tangential and any boundary-layer-control jets added to the chamber and is removed thru torque on the internal walls and flow thru the exhaust. Rather than attempt an exact computation involving all the terms in such a balance, we consider the boundary layer on the internal surface of the cylindrical wall. This is where most of the angular momentum is introduced into the chamber and where one of the most important losses occurs. The balance thru this boundary layer may be written as

$$\dot{m}_t \ v_t + \tau_\delta 2\pi\ell r_\delta = (\dot{m}_t + \dot{m}_r) \ v_0 + r_0 \ \ell \int_0^{2\pi} \tau_w \ d\theta \tag{12}$$

The second term on the left hand side is the torque exerted by the main vortex on the edge of the boundary layer. It represents a source of angular momentum for the boundary layer, but for large $\dot{m}_t/\mu\ell$ it is usually small compared with the other 3 terms and will be ignored here.

Our theoretical investigation of this boundary layer as a periodic wall jet, given in Appendix B, suggests that a reasonable approximation to τ_w may be based on the geometrical mean of the initial wall jet velocity, $\bar{v}$, and the final velocity, v_0.

$$\tau_w = \frac{C_f}{2} \ \rho_0 \ \bar{v} \ v_0 \tag{13}$$

15

Since the heavy particles or droplets will mix very rapidly with the entering wall jet, this mixing should occur with essentially no loss of jet momentum and the initial wall jet velocity may be taken as

$$\bar{v} = v_o + \sqrt{\rho_1/\rho_o} \ (v_t - v_o) \tag{14}$$

Correlations of losses in a single phase vortex show that Eq (13) and Eq (14) are reasonable when used in conjunction with the Blasius flat plate formula for C_{f_o} [5]

$$C_{f_o} = 0.072 \ (\rho_o \ v_o \ b/\mu)^{-0.2} \tag{15}$$

with b the circumferential distance between jets. Here, we assume that Eq (13), Eq (14) and Eq (15) are valid also for the two-phase vortex even when there are large differences between ρ_o and ρ_1. Also, we assume the effect of blowing can be accounted for by using correlations from flat plate data, (See for example Ref. 10). We will use

$$C_f = C_{f_o} \ (1 - B/2) \tag{16}$$

with a mass transfer number defined for this purpose as

$$B = \frac{\dot{m}}{\rho_o \ v_o \ A_w} \ \frac{2}{C_{f_o}} \tag{17}$$

as valid for $B \leq 1$.

With the above outlined approximations, Eq (12) may be solved for the recovery factor v_o/v_t to give

$$\frac{v_o}{v_t} = \frac{2 + \sqrt{\rho_1/\rho_o} \ (\dot{m}_r/\dot{m}_t)}{K + \left[K^2 + 2C_{f_o} \frac{\rho_o A_w}{\rho_1 A_t} (1 - \sqrt{\rho_1/\rho_o}) (1 + \frac{1}{2} \sqrt{\frac{\rho_1}{\rho_o}} \frac{\dot{m}_r}{\dot{m}_t}) \right]^{1/2}}$$

with $\hspace{10cm}$ (18)

$$K = 1 + \frac{\dot{m}_r}{\dot{m}_t} - \frac{1}{2} (1 - \sqrt{\rho_1/\rho_o}) \frac{\dot{m}_r}{\dot{m}_t} + \frac{1}{2} \sqrt{\rho_o/\rho_1} \ \frac{A_w}{A_t} C_{f_o}$$

This shows how the velocity in the chamber should decrease as ρ_o/ρ_1 and $\dot{m}_r/\dot{m}_t$ increase. This is compared with a somewhat more elaborate integral method solution in Appendix B, Fig. B6, and shown to be in rough agreement for $\dot{m}_r = 0$. It is plotted for various values of K as a function of $\dot{m}_r/\dot{m}_t$ in Figs. B7 and B8. Note that in the limit of $\rho_o/\rho_1 \to \infty$, $v_o/v_t \to (2\rho_1 A_t/ \rho_o A_w C_{f_o})^{1/2}$.

Rather than complete the angular momentum balance, we assume that the circulation is approximately constant between r_o and r_e. We expect this to be

16

particularly valid when there are large radial particle flows. This is not equivalent to ignoring losses on the end walls. Instead it assumes that the torque losses on the end walls are compensated by the BLC flow and the angular momentum defect existing in the end-wall boundary-layer flow. In this case

$$v_e = v_o \, r_o/r_e \qquad (19)$$

The consistency of our approximation can be checked by computing Δp from our theoretical velocity distribution and comparing with Fig. 9. In the limit of $\rho_o/\rho_i \to \infty$, Eq (1) and Eq (18) lead to

$$\lim_{\rho_o/\rho_i \to \infty} \Delta p \to \frac{\rho_i \, v_t^2 \, A_t}{C_{f_0} \quad A_w} \left[\left(\frac{r_o}{\bar{r}}\right)^2 - 1 \right]^{1/2} \qquad (20)$$

For the conditions of Fig. 9 ($\rho_i \, v_t^2 \cong 1.3$ in of Hg, $A_t/A_w = 0.0059$, and the Reynolds number appearing in Eq (15) is $\cong 5 \times 10^5$) and assuming the value of $\bar{r}/r_o = 0.7$ used in the last section, Eq (15) and Eq (19) give an asymptotic value of $\Delta p \cong 1.5$ in of Hg. This agrees even better with Fig. 9 than our assumptions would warrant.

With the above model of the flow, the restriction on containment given in Eq (11) may be written, using Eq (19) as

$$\frac{v_o}{v_i} \gtrsim \frac{3}{r_p} \frac{r_e}{r_o} \left[\frac{\mu A_t}{\rho_g \, v_t \, \ell} \frac{(1 + \dot{m}_r/\dot{m}_t)}{(\rho_s - \rho_g)} \right]^{1/2} \qquad (21)$$

and v_o/v_t eliminated between Eq (18) and Eq (21), to give limiting values of ρ_o/ρ_i for specified values of the other parameters.

These calculations show a variation of ρ_o/ρ_i with $\dot{m}_t/\dot{m}_r$ which is quite similar to that in the experimental curves of Figs. 6 and 7. The curves show numerical agreement if $r_p \cong 3$ microns (for $\dot{m}_t = 13$ gram/sec). We have not made any measurements of r_p yet, and theoretical modeling of the droplet formation process in the chamber is highly speculative. But, if formation is assumed to be controlled by a balance between the inertia of the liquid in the end wall boundary layers near the center of the chamber and surface tension then this value of $r_p = 3$ microns leads to reasonable values of the Weber number, $\rho v^2 r_p/\sigma$ (= 5 for $\rho = 1$ gm/cm^3, $\sigma = 60$ dynes/cm and $v = 10^3$ cm/sec). Thus the limits provided by Eq (18) and Eq (21) appear consistent with our experiments.

Heat transfer characteristics may be related to shear losses at the wall by assuming Reynold's analogy is valid. In this case

$$q_w \cong \frac{C_f}{2} \rho_o \, v_o \, (h_o - h_w) \, A_w \qquad (22)$$

with the subscript zero denoting conditions at the edge of the boundary layer. Equation (22) with the aid of Eq (12), (13) and (14) leads to

$$\frac{q_w}{(h_o - h_w)A_w} = \frac{\dot{m}_t}{A_w} \frac{[v_t/v_o - (1 + \dot{m}_r/\dot{m}_t)]}{[1 - \sqrt{\rho_1/\rho_o}\,(1 - v_t/v_o)]} \tag{23}$$

In a reactor q_w is limited to that which can be convected out by the gas passing thru it, i.e.

$$q_w = (\dot{m}_r + \dot{m}_t)\, h_w \tag{24}$$

and Eq (23) may be written as a limit on h_o/h_w

$$\frac{h_o}{h_w} - 1 = \frac{(1 + \dot{m}_r/\dot{m}_t)\,[1 - \sqrt{\rho_1/\rho_o}\,(1 - v_t/v_o)]}{[v_t/v_o - (1 + \dot{m}_r/\dot{m}_t)]} \tag{25}$$

This expression has already been used in the last section to estimate the liquid-wall interaction in the model experiment. It can also be used in conjunction with Eq (19) and Eq (20) to relate wall heat transfer to containment. The enthalpy h_o is that at the edge of the cylindrical wall boundary layer and thus provides a quite conservative estimate of the maximum temperature within the chamber. Since most of the fuel may be expected to be contained (and thus most of the energy generated) in an annulus in the main chamber rather than within the boundary layer T_{max} may be significantly higher than T_o.

6. CONCLUSIONS

The demonstration of containment of water in a small model with good interaction characteristics is naturally a long way from establishing the feasibility of containing hot uranium carbide dissolved in zirconium carbide with hydrogen as the gas in a full scale reactor. Yet, we can draw two conclusions from our results which are favorable to such a reactor concept.

First, containment of density ratios of $\rho_{av}/\rho_g \gtrsim 100$, as would probably be required for criticality, can be achieved over a range of operating conditions. The operating range may be even wider in the full scale case since σ and ρ_s/ρ may be expected to be substantially higher and Eq (21) indicates that containment should improve with increases in these parameters.

Second, the requirement for the capability of transferring 1/2 of the energy from the liquid directly to the gas should be achievable over a portion of the operating region within the containment envelope. In the model, the interaction between the liquid and gas was up to an order of magnitude larger than that between the liquid and the wall when interpreted as a conductance ratio.

SYMBOLS

A	area
C_f	coefficient of friction
C_h	heat transfer film coefficient
C_p	specific heat at constant pressure
C_s	mass transfer coefficient
h	enthalpy
ℓ	chamber length
$\dot{m}$	mass flow
q_w	heat transfer to the wall
r	radial coordinate
r_p	particle or droplet radius
r_p	inner radius of the annulus filled with the liquid-air mixture
S	interaction parameter defined in Eq (5)
T	temperature
v	tangential velocity
x	concentration of trace gas
Δp	pressure drop between the vortex centerline and r_o
μ	viscosity
ρ	density
ρ_{av}	mass in the chamber divided by chamber volume
ρ_s	density of particle or droplet
σ_s	liquid surface tension

Subscripts

e	conditions at the radius of the exhaust
g	gas conditions
i	chamber inlet conditions
ℓ	liquid conditions
o	conditions at the edge of the cylindrical wall boundary layer
t	tangential inlet conditions
w	cylindrical wall conditions

REFERENCES

1. <u>Proceedings of 2nd Symposium on Uranium Plasmas: Research and Applications</u>, held in Atlanta, Georgia, November, 1971, AIAA.

2. Turman, B. N. and Hasinger, S. H., "Experimental Studies of the Colloid Core Reactor Concept", <u>Second Symposium on Uranium Plasmas: Research and Applications</u> (1971).

3. Jackomis, W. N. and Von Ohain, H. J. P., "Aeromechanical Characteristics of Nuclear Reactor Cavities Using Colloidal Fuels", AIAA Paper No. 70-1222, October 1970.

4. Anderson, L. A., Hasinger, S. H. and Turman, B. N., "Two Component Vortex Studies with Implications for the Colloid Core Nuclear Rocket Concept", AIAA Paper No. 71-637, June 1971.

5. Lewellen, W. S., <u>A Review of Confined Vortex Flow</u>, NASA CR-1772, July 1971.

6. Tang, Y. S., Stefanko, J. S., Dickson, P. W., and Drawbaugh, D. W., "An Engineering Study of the Colloid-Fueled Reactor Concept", <u>Journal of Spacecraft and Rockets</u>, <u>8</u>, 129-132, February 1971.

7. Bradley, D., <u>The Hydrocyclone</u>, Pergamon Press, 1965.

8. Cox, P. J., "Liquid Containment Characteristics of a Gas-Driven Vortex", M.S. Thesis, Dept. of Aero. & Astro., MIT, September 1971.

9. Jones, W. P., "Heat Transfer Study of a Liquid Core Nuclear Rocket", M.S. Thesis, Dept. of Aero. & Astro., MIT, September 1971.

10. McLafferty, G. H., "Limitations on Gaseous Nuclear Rocket I_{sp} Due to Nozzle Coolant Requirements", <u>J. Spacecraft and Rockets</u>, <u>3</u>, 1515-1522, October 1966.

APPENDIX A

LIQUID-WALL CHEMICAL INTERACTION

Experiments were done using the concept of a chemical species transport measurement as an analogy of heat transfer to quantify the liquid-wall interation. Reactant selection was limited by available porous wall materials and liquid reactants. As with the gas-liquid measurements, prime desiderata was transport control of reaction rate and a unique quantitatively identifiable reaction product, in this case transported out as a gas with the exhaust. In our work, we chose to employ a porous copper wall of geometry similar to the nickel wall used for containment and gas-liquid interaction tests. This was based in large part on the availability of uniform low porosity copper sheet. Since some data was available on the reaction, we employed a nitric acid solution as the liquid phase reactant.

The net reaction expected is

$$3 \; Cu \; (s) + 8 \; HNO_3 \; (solu) \rightarrow 3 \; Cu \; (NO_3)_2 \; (solu) + 4 \; H_2O + 2 \; NO \quad (gas) \qquad (1)$$
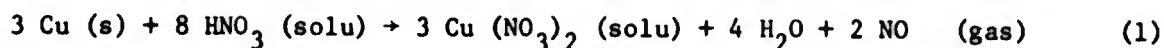
For transport control the production rate of NO is then

$$\dot{m}_{NO} = (C_s A)_w \; X_{HNO_3} \; (\ell) \cdot \frac{1}{4} \frac{M_{NO}}{M_{HNO_3}} \qquad (2)$$

and an analogous heat transfer rate across the wall boundary layer is

$$\dot{q}_w = (C_h A)_w \; (T_\ell - T_w) \qquad (3)$$

Assuming a definable T_ℓ constant through the liquid with the exception of the boundary layer, Eq (2) and Eq (3) give

$$\frac{\dot{q}_w}{\dot{m}_{NO}} = \frac{(C_h A)_w}{(C_s A)_w} \; \frac{T_\ell - T_w}{X_{HNO_2}(\ell)} \; \frac{4 \; M_{HNO_3}}{M_{NO}}$$

$$= Le_{\ell - w} \; \frac{Cp(T_\ell - T_w)}{X_{HNO_3}(\ell)} \; \frac{4M_{HNO_3}}{M_{NO}} \qquad (4)$$

The Lewis number defined here is not necessarily near unity since the nuclear fuel may have significant heat conduction by electron motion. In the case of a highly turbulent field this effect would be unimportant and Le ≈ 1.

An estimate of the species transport rate from liquid to wall can be obtained by use of a unity Lewis number assumption and Eq (5), from the text as

$$(C_s A)_w = (C_h A)_w \; \frac{1}{Cp \; Le} = \frac{\dot{m}}{S} \qquad (5)$$

21

In Eq (2) this gives

$$\dot{m}_{NO} = \frac{\dot{m}}{S} \, X_{HNO_3}(\ell) \, \frac{1}{4} \, \frac{M_{NO}}{M_{HNO_3}} \tag{6}$$

For our experimental conditions, this predicts a NO production rate of approximately 1 gram per second at $X_{HNO_3}(\ell) = 0.49$. We observed less than 10^{-2} gram per second. At acid concentrations of $X_{HNO_3}(\ell) = 0.02$ to 0.4, no measurable product was found. Also, the total mass of copper lost from the porous wall is close to that which the stoichiometry reaction, Eq (1) predicts for the total HNO_3 input used.

From this data it appears that the reaction proceeded very slowly, subject to chemical kinetic rate control. This is expressed as

$$\dot{m}_{NO} = X_R \, Ae^{-E/RT_w} \tag{7}$$

where X_R is the concentration at the wall of the species which reacts with the copper. This is consistent with the observed rate of reaction in the high concentration case. It also allows interpretation of the observation that NO production was highly nonlinear with respect to HNO_3 concentration, in terms of the classical ignition-extinction balance of exothermic reaction with heat transfer.* Time delays inherent in emptying and cleaning the apparatus were adequate for complete reaction of the HNO_3, even at the observed low rates.

It was, of course, intended that the reaction of Eq (1) be transport controlled. From Eq (6) it is clear that this transport is a very fast process, with a time scale to transport all reactant to the wall of

$$\tau_{xport} \sim S \, M_\ell \big/ \dot{m} \sim 5 \text{ seconds}$$

While this estimate is clearly highly approximate it appears that observed kinetic reaction rates are about two orders of magnitude too slow for our purposes. Use of either a highly reactive chemical system, with steady reactant injection, or of a direct heat transfer measurement scheme appears to be necessitated.

---

*Frank-Kaminetskii, D. A., Diffusion and Heat Exchange in Chemical Kinetics, Princeton University Press, Princeton, New Jersey, 1955.

APPENDIX B

TWO PHASE FLOW IN THE CYLINDRICAL
WALL BOUNDARY LAYER

1. INTRODUCTION

The purpose of the present investigation is to study the two phase boundary layer flow in a confined vortex chamber. Knowledge of such a flow field has immediate engineering application to colloid core nuclear reactor rocket engines. Within the time limit of the present study a thorough analysis of the flow problem is deemed not possible. We singled out the recovery factor, U_o/U_1, as one of the most significant parameters of the problem. The dependence of this parameter on the ratio of particle density to gas density in the vortex, turbulence level in the wall layer, wall jet characteristics etc. is the subject of this Appendix.

The problem to be analyzed consists of a cylindrical vortex chamber. Fluid is injected tangentially into the chamber through slits spaced regularly along the chamber wall. In this work we will initially assume that the wall is solid without radial wall injection. However, the mathematical model which will be developed in the next section is extended in the final section to allow for this possibility. The tangentially injected fluid sets up a swirling flow inside the chamber. The interaction of this swirling flow and the wall boundary gives rise to a periodic wall boundary layer. In the proposed colloid core nuclear reactor rocket engine fuel in the form of small solid particles are suspended in the vortex flow. Because of centrifugal force these particles tend to migrate toward the chamber wall forming a thick dusty layer there. The presence of these particles alters the boundary-layer thickness, the shear stresses on the chamber wall and hence the recovery factor.

Figure (B-1) is a sketch of the flow field of the boundary layer. Depending on whether the Reynolds number is small or large the flow can be laminar as well as turbulent. The structure of the flow is governed by the wall jet and the periodic boundary conditions at $x = 0$ and $x = \ell$ as shown in Fig. (B-1). In going downstream of an injection slit along the chamber wall the velocity profile of the boundary layer is chiefly in the form of a jet. The width of the jet broadens out and the maximum velocity of the jet diminishes as the boundary layer evolves downstream until close to the next injection slit where the jet profile becomes no longer recognizable. On reaching the next jet a typical boundary layer profile emerges. Further downstream the flow field repeats itself so that we can simply restrict our analysis to one period of the flow.

Early in this study it was recognized that there was little experimental data available for comparison with the present calculation. It was felt that to insure the model to be used in the calculation is reasonably sound, the case without particles should first be analyzed and comparison with existing data and calculations be made. Also in studying the simpler model without particles some insight into the physics of the problem could be gained. Accordingly, in sections 2 and 3 of this report the cases without particles will first be examined. When the flow Reynolds number is small, the boundary layer is laminar. This laminar case has been investigated by Keyes, Chang and Sartory[B.1] both experimentally and theoretically. In their theoretical work the boundary layer equation with appropriate boundary and periodic conditions was solved by means of a finite difference scheme on a computer. A good deal of computer time was found necessary (several hours)
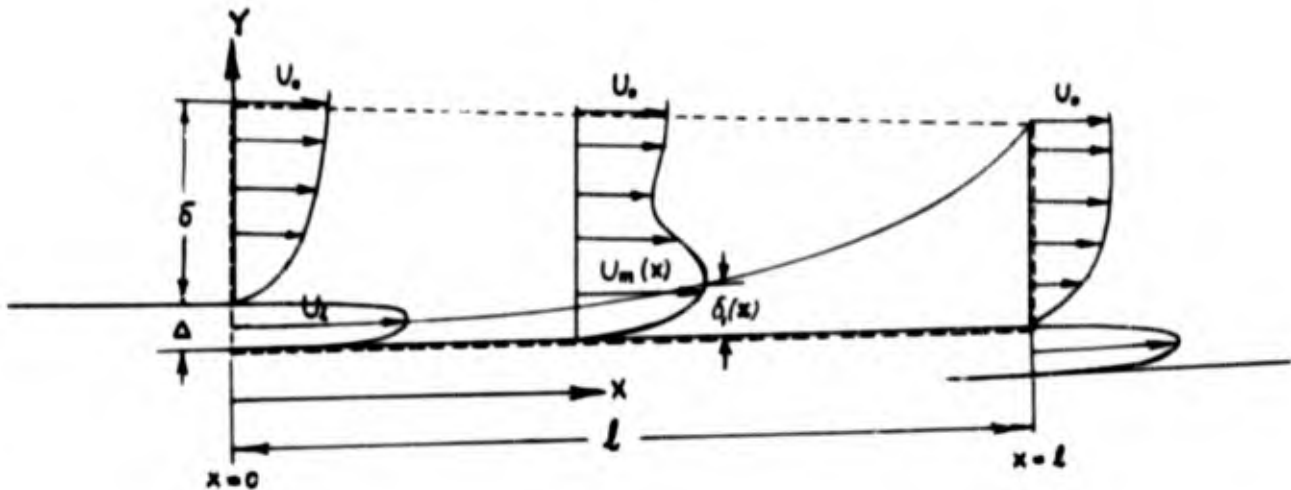
Fig. B-1 Two-Dimensional Idealization of the Cylindrical
Wall Boundary Layer

when the recovery factor of the flow is small. On comparing with experiments the theoretical results are excellent. However, computer solutions like their work do not provide insight and understanding to the problem which we badly need in order to deal with the turbulent case and the two-phase boundary layer. Experimental data, when the boundary layer is turbulent, are available in the literature. But the data have a good deal of scatter[B.2,B.3]. No undisputed theoretical calculation exists in the turbulent case. With certain empirical assumptions formulas for estimating the recovery factor have been given by Roschke[B.4], Felsing, Mockenhaupt and Lewellen[B.5] and others. In sections 2 and 3 the results of our model will be used to compare with these works.

In the course of this study it is found that the lower layer of the wall jet (layer below the point of maximum velocity of the jet profile) which we shall call the wall layer plays a decisive role in determining the recovery factor of the vortex flow. In fact, by using a simple but reasonable model of this layer alone a good estimate of the recovery factor is possible. Dynamically one can interpret this as suggesting that the outer layer is of secondary importance. To see that this assertion is true let us consider the case when the flow is laminar. Figure (B-2) shows the development of the wall layer. In many respects one readily sees that the wall layer cannot be too far from that of laminar boundary layer flow past a flat plate. The principle difference is that for the wall layer the free stream velocity $U_m(x)$ varies spatially. At $x = 0$, $U_m(x)$ is equal to the injection velocity U_1 and at $x = \ell$, $U_m(x)$ is equal to the free streaming velocity U_0. If the recovery factor U_0/U_1 is close to unity, it is clear that for the purpose of estimating the shear stress at the wall a good approximation is to take $U_m(x)$ to be a constant equal to some mean value between U_1 and U_0. There is no way to choose which mean value to use but the arithmetic mean $\bar{U} \triangleq (U_0 + U_1)/2$ and the geometrical mean $\tilde{U} = \sqrt{U_0 U_1}$ are not unreasonable.
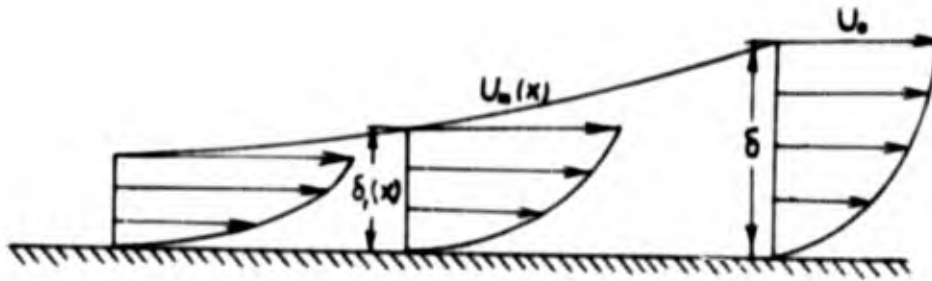
24

Fig. B-2 Wall Layer

From Blasius' solution of boundary layer over a flat plate, with the above approximation, we find that the total force on the wall, D, is

$$D = \int_0^l \tau_w(x)dx = \int_0^l 0.332\mu \; \bar{U}\sqrt{\frac{\bar{U}}{\nu x}} \; dx = 0.664 \; \bar{U}\sqrt{\mu\rho l\bar{U}} \tag{B.1}$$

Now let us consider the balance of x-momentum of the fluid in the control volume shown in Fig. (B-1). If m and q denote the momentum and volume flux of the slit jet, then to conserve x-momentum we have,

$$m = \rho q U_o + D \tag{B.2}$$

where ρ is the density of the fluid. We will define the recovery factor U_o/U_1 by $U_o/U_1 = \rho U_o q/m$. The work of Keyes, Chang and Sartory[B.1] shows that the recovery factor U_o/U_1 is a unique function of a dimensionless parameter $\bar{w} = q/\sqrt{U_1 \nu l}$ where l is the distance between slits. Now on substituting Eq (1) into Eq (2) a relation between the recovery factor and $\bar{w}$ can be found. If $\bar{U} = (U_1 + U_o)/2$ is used we have

$$\frac{U_1}{U_o} = 1 + \frac{0.664}{\bar{w}} \left(\frac{U_1 + U_o}{2U_o}\right)^{3/2} \left(\frac{U_o}{U_1}\right)^{1/2} \tag{B.3}$$

If $\bar{U} = \sqrt{U_1 U_o}$ is used, we obtain

$$\frac{U_1}{U_o} = 1 + \frac{0.664}{\bar{w}} \left(\frac{U_1}{U_o}\right)^{1/4} \tag{B.4}$$

A comparison between Eq (3) and Eq (4) and the computer result of Keyes, Chang and Sartory is given in Fig.(B-3). In this figure the curve labelled (0) is the

25

computer result. The curve labelled (1) is a plot of Eq (3) while the curve labelled (2) is that of Eq (4). It is clear from these curves that the present approximate result, especially Eq (4) is a good approximation for almost the entire range of recovery factor. This rather surprising result not only confirms our earlier assertion but also shows (a) that the wall layer is similar to that of boundary layer over a flat plate and (b) that assuming $U_\infty(x)$ to have a mean constant value is a good approximation insofar as calculating the wall shear stress is concerned.
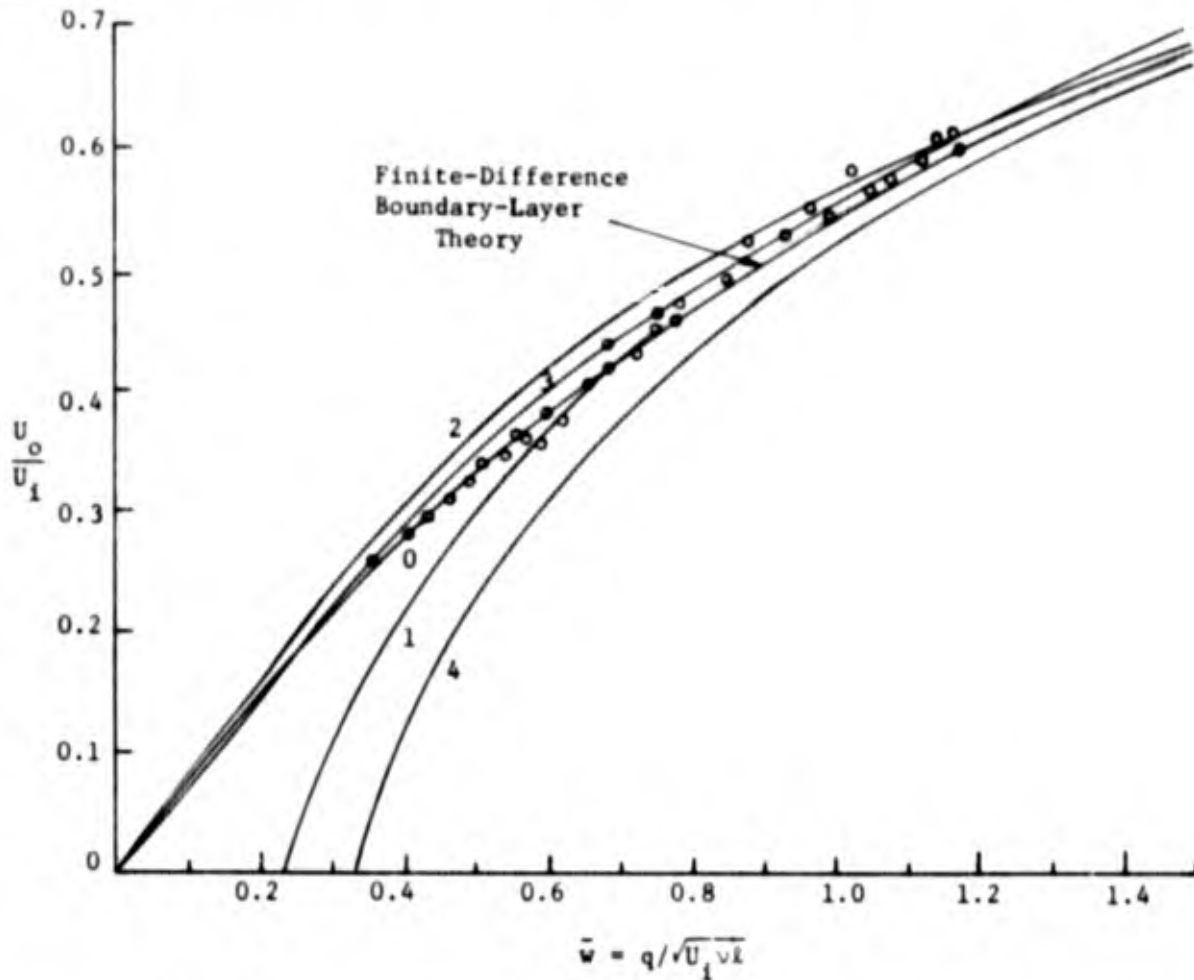
Fig. B-3 Recovery Factor for a Laminar Boundary Layer. Zero Curve and Data from Keyes, Chang and Sartory, 1967. [(1)-Eq (3), (2)-Eq (4), (3)-Eq (21) and Eq (22) with $\bar{U}' = \sqrt{U_1/U_0}$, and (4)-Eq (21) and Eq (22) with $\bar{U}' = (1 + U_1/U_0)/2$].

In section 2 of this report the laminar vortex boundary layer will be studied in some detail. A two-layer model of the flow field using the well known momentum integral technique will be developed. In section 3 the case of a turbulent boundary layer is dealt with. A suggestion as to how the effect of turbulence can be accounted for is proposed. Finally, in section 4 and 5, the case of two-phase boundary layer flow is studied.

2. THE LAMINAR CASE

When the boundary layer flow is laminar the flow in the injection slit must also be laminar. Thus at $x = 0$, Fig. (B-1), the jet profile is parabolic. From this it is easy to find that

$$m \text{ (momentum flux of jet)} = \rho \int_0^\Delta U^2 dy \Big|_{x=0} = \frac{8\rho}{15} \Delta U_j^2 \tag{B.5}$$

$$q \text{ (volume flux of jet)} = \int_0^\Delta U dy \Big|_{x=0} = \frac{2}{3} \Delta U_j \tag{B.6}$$

$$\frac{U_c}{U_j} \text{ (recovery factor)} = \frac{U_o \rho q}{m} = \frac{U_o}{0.8 U_j} \tag{B.7}$$

where Δ is the width of slit and U_j is the maximum velocity of the jet.

Let us now divide the boundary layer flow into two layers, namely, the wall layer and the outer layer as shown in Fig. (B-1). These two layers can be treated separately by the well known momentum integral technique. For this purpose one can regard the total boundary layer thickness, δ, as constant and take $U_m(x)$ and $\delta_1(x)$ as the profile parameters. If U and v denote the velocity components in the x and y directions respectively, then the boundary layer equations are:

$$\frac{\partial U}{\partial x} + \frac{\partial v}{\partial y} = 0 \tag{B.8}$$

$$U \frac{\partial U}{\partial x} + v \frac{\partial U}{\partial y} = \frac{1}{\rho} \frac{\partial \tau}{\partial y} \quad , \, p \sim \text{constant} \tag{B.9}$$

By integrating Eq (9) from 0 to δ and using Eq (8) to eliminate v, it is straightforward to obtain,

$$\frac{d}{dx} \int_0^\delta (U^2 - U_o U) dy = -\frac{1}{\rho} \tau_w \tag{B.10}$$

(τ_w = shear stress at wall). Similarly by integrating Eq (9) from 0 to δ_1, we obtain

$$\frac{d}{dx} \left(\int_0^{\delta_1} U^2 dy \right) - U_m \frac{d}{dx} \left(\int_0^{\delta_1} U dy \right) = -\frac{1}{\rho} \tau_w \tag{B.11}$$

On subtracting Eq (11) from Eq (10) we find

$$\frac{d}{dx} \left(\int_{\delta_1}^{\delta} U^2 dy \right) - (U_o - U_m) \frac{d}{dx} \left(\int_o^{\delta} U dy \right) - U_m \frac{d}{dx} \left(\int_{\delta_2}^{\delta} U \omega y \right) = 0 \qquad (B.12)$$

Let us introduce the following dimensionless variables

$$X = x/\ell \quad , \; Y = y/\delta \quad , \; \bar{U}(x,y) = U(x,y)/U_o$$

In terms of these dimensionless variables Eq (11) and Eq (12) can be rewritten as

$$\frac{d}{dX} \left(\int_o^{\bar{\delta}_1(x)} U^2 dY \right) - \bar{U}_m \frac{d}{dx} \left(\int_o^{\bar{\delta}_1(x)} \bar{U} dY \right) = - \left(\frac{\partial \bar{U}}{\partial Y} \right)_{Y=0} \left(\frac{\ell}{\delta R_\delta} \right) \qquad (B.13)$$

$$\frac{d}{dX} \left(\int_{\bar{\delta}_1(x)}^{1} \bar{U}^2 dY \right) - (1 - \bar{U}_m(X)) \frac{d}{dX} \left(\int_o^{1} \bar{U} dY \right) - \bar{U}_m \frac{d}{dX} \left(\int_{\bar{\delta}_1}^{1} \bar{U} dY \right) = 0 \qquad (B.14)$$

The appropriate boundary conditions are

$$\bar{U}_m(0) = U_j/U_o, \qquad \bar{U}_m(1) = 1 \qquad (B.15)$$

$$\bar{\delta}_1(0) = \Delta/2\delta, \qquad \bar{\delta}_1(1) = 1 \qquad (B.16)$$

$(R_\delta = U_o \delta / \nu)$. In principle, Eq (13) and Eq (14) together with boundary conditions Eq (15) and Eq (16) provide a unique solution to the problem and two relations between the three parameters of the problem i.e. $\ell/\delta R_\delta$, U_j/U_o and $\Delta/2\delta$. However, as shown in section 1 if U_j/U_j, the recovery factor is the quantity of prime interest, an estimate of its dependence on other quantities can be obtained by assuming $U_m(x)$ to be constant. Here we shall use this simplifying assumption. If $U_m(x)$ is a constant, only Eq (11) is needed. However, in order to provide two relations for the three parameters $\ell/\delta R_\delta$, U_j/U_o, and $\Delta/2\delta$, one additional condition other than that of Eq (16) is necessary. This can be obtained by integrating Eq (10) from 0 to ℓ which is just the condition of balance of x-momentum as employed in section (1)

$$m = \rho q U_o + \int_o^{\ell} \tau_w dx \qquad (B.17)$$

Specifically, let us now take the velocity profile of the wall layer to be

$$U = \frac{1}{2} U_m (3\eta - \eta^3) \qquad , \; \eta = y/\delta_1 \qquad (B.18)$$

28

Then from Eq (13), Eq (16) and Eq (17) we obtain (after using Eq (5) and Eq (6))

$$\frac{17}{35} \frac{d}{dX} (\bar{U}_m^2 \bar{\delta}_1) - \frac{5}{8} \bar{U}_m \frac{d}{dX} (\bar{U}_m \bar{\delta}_1) = - 1.5 \frac{\bar{U}_m}{\bar{\delta}_1} (\frac{\ell}{\delta R_\delta})$$

$$\bar{\delta}_1(0) = \frac{\Delta}{2\delta} \quad , \quad \bar{\delta}_1(1) = 1 \tag{B.19}$$

$$\frac{2}{3} (\frac{\Delta}{\delta}) (\frac{U_1}{U_o}) [0.8 (\frac{U_1}{U_o}) - 1] = 1.5 \frac{\ell}{\delta R_\delta} \int_o^1 \frac{\bar{U}_m}{\bar{\delta}_1} dX$$

where from Eq (7), $U_j/U_o = 0.8 \, U_1/U_o$.

Now with $\bar{U}_m = \tilde{U}'$ (constant), Eq (19) can be integrated to give

$$\bar{\delta}_1(X) = \left[(1 + \frac{21.539}{\tilde{U}'})(\frac{\ell}{\delta R_\delta}) (X - 1) \right]^{1/2} \tag{B.20}$$

The two relations among the three parameters of the problem are found to be

$$\frac{\Delta}{25} = [1 - \frac{21.539}{\tilde{U}'} \frac{\ell}{\delta R_\delta}]^{1/2} \tag{B.21}$$

$$\frac{2}{3} (\frac{\Delta}{\delta}) (\frac{U_1}{U_o})(0.8 \frac{U_1}{U_o} - 1) - \frac{39}{280} \vec{U}^2 (1 - \frac{\Delta}{2\delta}) = 0 \tag{B.22}$$

Equation (21) and Eq (22) have been solved for the cases (a) $\tilde{U}' = (1 + U_j/U_o)/2$, and (b) $\tilde{U}' = \sqrt{U_j/U_o}$. The dependence of recovery factor U_o/U_1 on $\bar{w}$ is shown as curve (4) and curve (3) in Fig. (B-3). It is seen that they approximate the exact computer solution very well especially curve (3). Encouraged by the success and simplicity of the assumption $U_m \simeq \sqrt{U_o U_j}$ (constant) in this case, we will use this approximation throughout the rest of this Appendix.

3. THE TURBULENT CASE

The main difficulty of considering the turbulent case is how to account for the turbulent characteristics of the flow in the calculation of the recovery factor. In the two layer model proposed in section 2 a natural way to take this effect into account is to take τ_w as that given by the (turbulent) Blasius formula for flow over a flat plate. That is

$$\tau_w = 0.0225 (\frac{\nu}{U_m \delta_1})^{1/4} \rho U_m^2 \tag{B.23}$$

Of course, strictly speaking, this is incorrect. But physically it is certainly a good approximation.

To see how good this formula is in the present problem let us proceed as in the laminar case to obtain an estimate on the recovery factor U_o/U_i and compare this result with experimental values. By using a 1/7th power velocity profile and wall shear stress formula as in Eq (23) we obtain from Schlichting[B.6] the following drag formula on the wall.

$$\text{Drag} = D = 0.036 \ \rho \tilde{U}^2 \ell \ \left(\frac{\tilde{U}\ell}{\nu}\right)^{-1/5} \tag{B.24}$$

Here $\tilde{U}$ is a mean value of $U_m(X)$. From balance of x-momentum in the control volume shown in Fig. (B-1) we have

$$m = \rho q U_o + 0.036 \ \rho \tilde{U}^2 \ell \ \left(\frac{\tilde{U}\ell}{\nu}\right)^{-1/5} \tag{B.25}$$

For a turbulent jet, for all intents and purposes, we have

$$m = \rho U_i^2 \ \Delta$$

$$q = U_i \Delta$$

On substituting into Eq (25) the following formulas for the recovery factor are obtained.

(a) $\tilde{U} = (U_o + U_i)/2$

$$\frac{\ell}{\Delta} \ \frac{1}{\left[\frac{U_o \ell}{\nu}\right]^{1/5}} = \frac{(1 - \frac{U_o}{U_i})(1 + \frac{U_o}{U_i})^{0.2}}{0.0104 \ (1 + \frac{U_o}{U_i})^2 \ (\frac{U_o}{U_i})^{0.2}} \tag{B.26}$$

(b) $\tilde{U} = \sqrt{U_o U_i}$

$$\frac{\ell}{\Delta} \ \frac{1}{(\frac{U_o \ell}{\nu})^{1/5}} = \frac{1 - \frac{U_o}{U_i}}{0.036 \ (\frac{U_o}{U_i})^{1.1}} \tag{B.27}$$

Figure (B-4) shows a plot of Eq (26) and Eq (27). For sufficiently large recovery factor the two curves are about the same. Considerable difference exists when U_o/U_i is small. This is also true in the laminar case as can be seen in Fig. (B-3). We believe that this large difference is because $\tilde{U} = 0.5 \ (U_o + U_i)$ is not a good approximation for small recovery factor.

In Fig. (B-5) we compare Eq (26) and Eq (27) with the experimental data of Rodoni (1969). Rodoni gave U_o/U_i as a function of the ratio of wall area to jet injection area (ℓ/Δ). Since the effect of kinematic viscosity, ν, is not
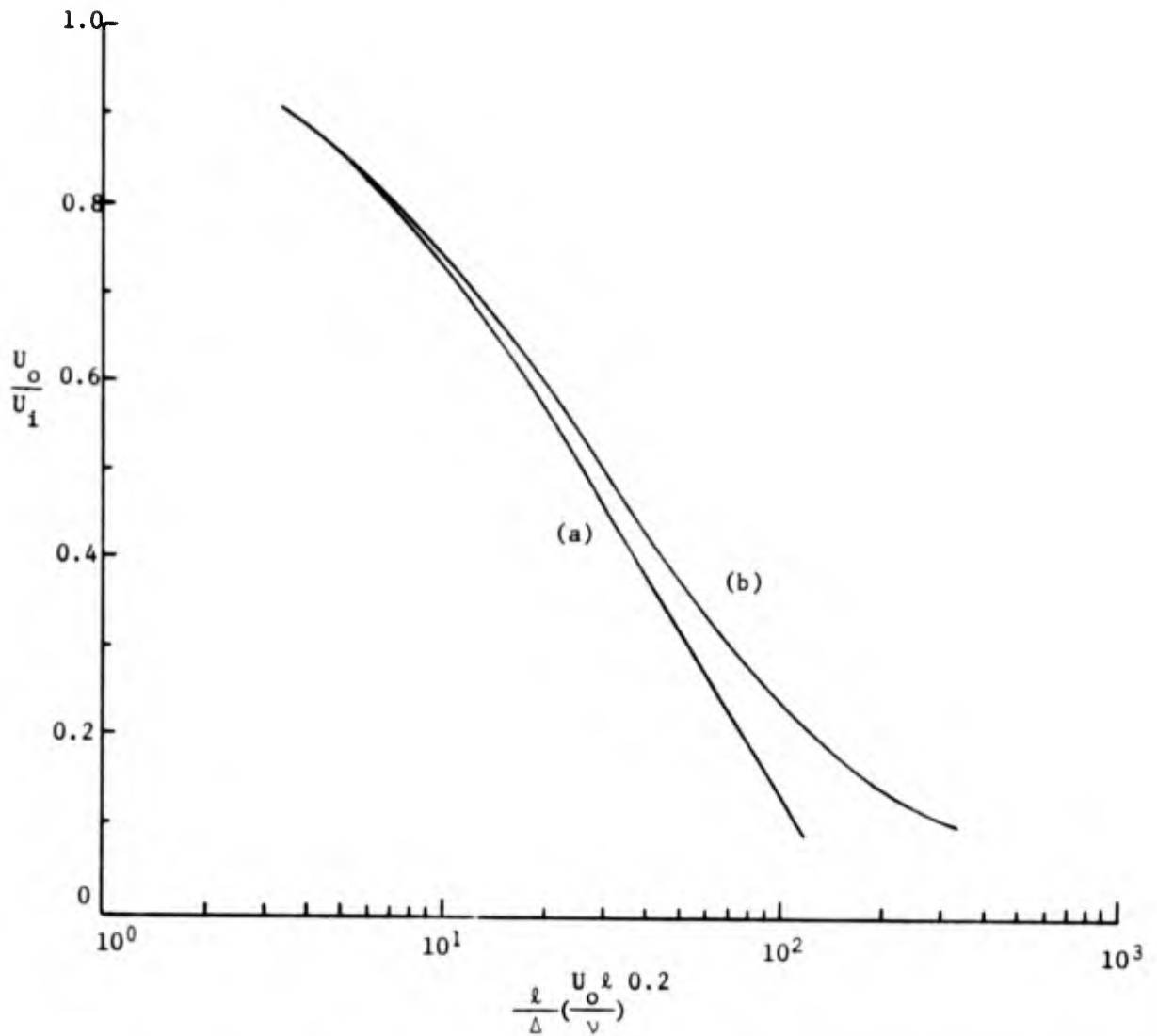
Fig. B-4   Recovery Factor, Turbulent Boundary Layer

incorporated into these variables the data show a bit of scattering as expected. To compare his data with Eq (26) and Eq (27) the factor $(U_o \ell/\nu)^{0.2}$ has been chosen to be equal to 13.0.   Curve (b) i.e. Eq (27) fits the data quite well for almost the full range of recovery factor. Curve (a) is a good fit for $U_o/U_1 > 0.4$. The dotted curve in Fig. (B-5) is given by Felsing, Mockenhaupt and Lewellen[B.5] who derived their results through a quasi-one-dimensional approximation. Equation (27) agrees fairly well with their curve.

From the above we note that the simple approximation of treating the wall layer alone by taking $U_m(X)$ to be a constant equal to $\sqrt{U_o U_1}$ together with the use of the (turbulent) Blasius formula Eq (23) for the flow over a flat plate does give reasonably good results for the full range of recovery factor. In the next section this information will be used to deal with the two phase flow problem.
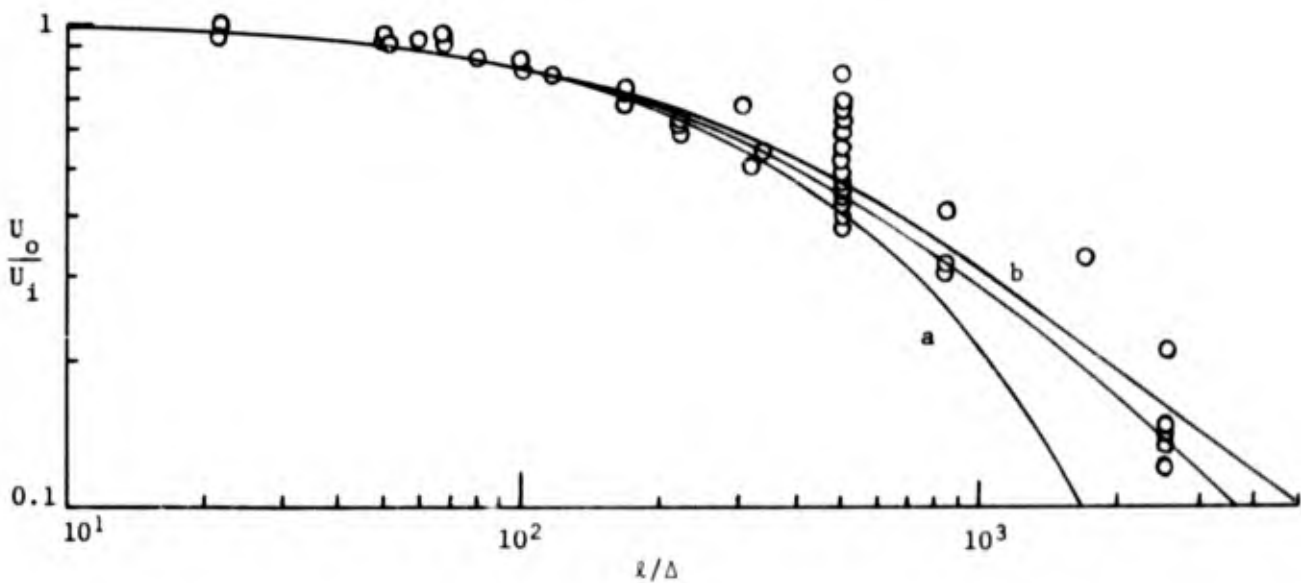
31

Fig. B-5 Recovery Factor as a Function of the Ratio of Wall Area to Injection Area (a: $\tilde{U} = (U_o + U_i)/2$; b: $\tilde{U} = \sqrt{U_o U_i}$). Data from Rodoni, 1969.

4. TWO PHASE BOUNDARY LAYER

The addition of particles into the boundary layer introduces several new effects into the problem. Two of these effects will now be briefly discussed. First is the density effect. For practical purposes the ratio of particle density to gas density in a colloid core nuclear reactor rocket engine will be very high, of the order of 100. Thus the composite fluid is very dense. Because of this high density the wall shear stress will be very large as compared with the pure gas case. The result of this is a huge loss of tangential momentum leading to a very small recovery factor. Second is the centrifugal force effect. Let us remember that the particles and fluid are actually moving more or less tangentially inside a cylindrical chamber of radius R. Owing to their large density, centrifugal force will tend to cause the particles to move radially outward. Of course, this tendency must be balanced somehow by the drag on these particles produced by the radially inward motion of the fluid. Inside the boundary layer close to the cylindrical chamber wall the distribution of centrifugal force due to the particles is not uniform on account of the variation of tangential velocity. This nonuniform distribution of centrifugal body force produces a spatial pressure gradient which could exert a strong influence on the boundary layer flow.

Inside the two-phase boundary layer a proper set of governing equations for most practical cases is:

Fluid Equations

$$\frac{\partial U}{\partial x} + \frac{\partial v}{\partial y} = 0 \qquad\qquad (B.28)$$

32

$$\rho\left(U\frac{\partial U}{\partial x} + v\frac{\partial U}{\partial y}\right) = -\frac{\partial p}{\partial x} + \frac{\partial \tau}{\partial y} - \rho_p \alpha\,(U - U_p) \qquad (B.29)$$

$$-\frac{\partial p}{\partial y} - \rho_p \alpha\,(v - v_p) = 0 \qquad (B.30)$$

Particle Equations

$$\frac{\partial \rho_p U_p}{\partial x} + \frac{\partial \rho_p v_p}{\partial y} = 0 \qquad (B.31)$$

$$U_p \frac{\partial U_p}{\partial x} + v_p \frac{\partial U_p}{\partial y} = \alpha(U - U_p) \qquad (B.32)$$

$$U_p \frac{\partial v_p}{\partial x} + v_p \frac{\partial v_p}{\partial y} = \alpha(v - v_p) - \frac{U_p^2}{R} \qquad (B.33)$$

where ρ_p, U_p, v_p are the particle density and velocity components in the x and y directions respectively. $\alpha = 9\mu/2\rho_s \sigma^2$ for small particles of radius σ and solid density ρ_s according to Stoke's drag formula.

If the size of particles is small ($\sigma \to 0$), the viscous drag terms in the particle momentum equations dominate over the inertia and centrifugal force terms. This is true in the proposed colloid core nuclear reactor rocket engine. In this case a good approximate solution to Eq (32) and Eq (33) is

$$U_p \simeq U \qquad (B.34)$$

$$v_p \simeq v$$

(However, this does not mean that the terms $\rho_p \alpha(U - U_p)$, $\rho_p \alpha(v - v_p)$ in Eq (29) and Eq (30) can be neglected. Actually if $\rho_p \gg \rho$ the term $\rho_p \alpha(U - U_p)$ is much more important than the fluid inertia terms on the left hand side). This permits us to rewrite Eq (31), Eq (32) and Eq (33) as

$$\frac{\partial(\rho_p U)}{\partial x} + \frac{\partial(\rho_p v)}{\partial y} = 0 \qquad (B.35)$$

$$U\frac{\partial U}{\partial x} + v\frac{\partial U}{\partial y} = \alpha(U - U_p) \qquad (B.36)$$

$$\alpha(v - v_p) = \frac{U^2}{R} \qquad (B.37)$$

By combining Eq (28), Eq (29) and Eq (30) with Eq (35), Eq (36) and Eq (37) the governing equations can be simplified to:

$$\frac{\partial U}{\partial x} + \frac{\partial v}{\partial y} = 0;$$

$$(\rho_p + \rho) \ (U \ \frac{\partial U}{\partial x} + v \ \frac{\partial U}{\partial y}) = - \frac{\partial p}{\partial x} + \frac{\partial \tau}{\partial y} \qquad (B.38)$$

$$- \frac{\partial p}{\partial y} = \rho_p \ \frac{U^2}{R}$$

$$\frac{\partial (\rho_p U)}{\partial x} + \frac{\partial (\rho_p v)}{\partial y} = 0$$

In the following we will restrict our considerations to cases where $\delta/R \ll 1$ and $\rho_p \simeq$ constant (inside the boundary layer) are approximately true. That is to say, we will neglect the effect of centrifugal force and the variation of particle density inside the two-phase boundary layer. Later models may permit a variation in ρ_p. With these approximations Eq (38) reduces to

$$\frac{\partial U}{\partial x} + \frac{\partial v}{\partial y} = 0$$

$$\rho (1 + \kappa) \ (U \ \frac{\partial U}{\partial x} + v \ \frac{\partial U}{\partial y}) = \frac{\partial \tau}{\partial y} \qquad (B.39)$$

$(\kappa = \rho_p/\rho)$. Equation (39) is similar to the turbulent case treated in section (3) and hence the method outlined in section (2) can now be used.

By integrating the second equation of (39) over y from 0 to $\delta_1(x)$ the integral momentum equation for the wall layer is found to be

$$\rho (1 + \kappa) \ [\frac{d}{dx} \ (\int_0^{\delta_1} U^2 dy) - U_m \frac{d}{dx} \ (\int_0^{\delta_1} Udy)] = - \tau_w \qquad (B.40)$$

To estimate the turbulent wall stress, τ_w, we can use Eq (23) with appropriate modification on the density of the fluid i.e.

$$\tau_w \simeq 0.0225 \ (\frac{\nu}{U_m \delta_1})^{1/4} \rho (1 + \kappa)^{3/4} U_m^2 \qquad (B.41)$$

Let us take the velocity profile in the wall layer to be

$$U = U_m \ (2\eta - 2\eta^3 + \eta^4) \ , \quad \eta = y/\delta_1$$

(a 1/7th power velocity distribution could be used but numerically there is not much difference). Since we are assuming that the particles mix immediately with the jet, with no loss of jet momentum, the initial wall jet velocity is taken to be $U_0 + (U_1 - U_0)/\sqrt{1 + \kappa}$. Thus the appropriate average value to use for U_m will be

34

assumed to be

$$U_m = \sqrt{U_o \left(U_o + \frac{U_1 - U_o}{\sqrt{1 + \kappa}}\right)} \qquad (B.42)$$

On substituting Eq (41) and Eq (42) into Eq (40) we obtain in terms of dimensionless variables introduced in section 2 the following equation for δ_1 (X)

$$0.118 \, \tilde{U}^2 \frac{d\bar{\delta}_1}{dX} = 0.0225 \frac{\tilde{U}^{7/4}}{\bar{\delta}_1^{1/4}} \frac{1}{(1 + \kappa)^{1/4}} \left(\frac{\ell}{\delta R_d^{1/4}}\right) \qquad (B.43)$$

where $\tilde{U} = [1 + (U_1 - U_o)/U_o \sqrt{1 + \kappa}]^{1/2}$. The boundary conditions are

$$\bar{\delta}_1(1) = 1 \qquad\qquad \bar{\delta}_1(0) = \frac{\Delta}{2\delta} \qquad (B.44)$$

The condition of balance of x-momentum is

$$\Delta \left(\frac{U_1}{U_o}\right) \left(\frac{U_1}{U_o} - 1\right) = \frac{1}{\rho U_o^2} \int_0^\ell \tau_w \, dx \qquad (B.45)$$

A solution of Eq (43) which satisfies the first condition of Eq (44) is

$$\bar{\delta}_1(X) = \left[\frac{0.238}{\tilde{U}^{1/4}(1 + \kappa)^{1/4}} \left(\frac{\ell}{\delta R_\delta^{1/4}}\right) (X - 1) + 1\right]^{4/5} \qquad (B.46)$$

By requiring Eq (46) to satisfy Eq (45) and the second condition of Eq (44), we obtain

$$\frac{\Delta}{2\delta} = \left[1 - \frac{0.238}{\tilde{U}^{1/4}(1 + \kappa)^{1/4}} \left(\frac{\ell}{\delta R_\delta^{1/4}}\right)\right]^{4/5} \qquad (B.47)$$

$$\frac{\Delta}{\delta} \left(\frac{U_1}{U_o}\right) \left(\frac{U_1}{U_o} - 1\right) = 0.118 \, \tilde{U}^2 (1 + \kappa)[1 - \frac{\Delta}{2\delta}] \qquad (B.48)$$

From Eq (47) and Eq (48) the dependence of the recovery factor (U_o/U_1) on the physical variables of the problem i.e. ℓ, Δ, U_1, ν and κ can be found. (Actually, Eq (47) and Eq (48) provide two relationships for the three dimensionless quantities, U_o/U_1, Δ/δ and ℓ/Δ $(U_1 \ell/\nu)^{0.2} = T$. Figure (B-6) shows the dependence of the recovery factor on the parameter T for various particle loading (κ). The case $\kappa = 0$ corresponds to the turbulent case examined in section 3. This curve agrees very well with curve (b) in Fig. (B-4).

The effect of particle loading on the recovery factor can be clearly seen in Fig. (B-6). Suppose we keep the injection velocity constant but continue to increase the density of particles in the boundary layer. In Fig. (B-6) this is
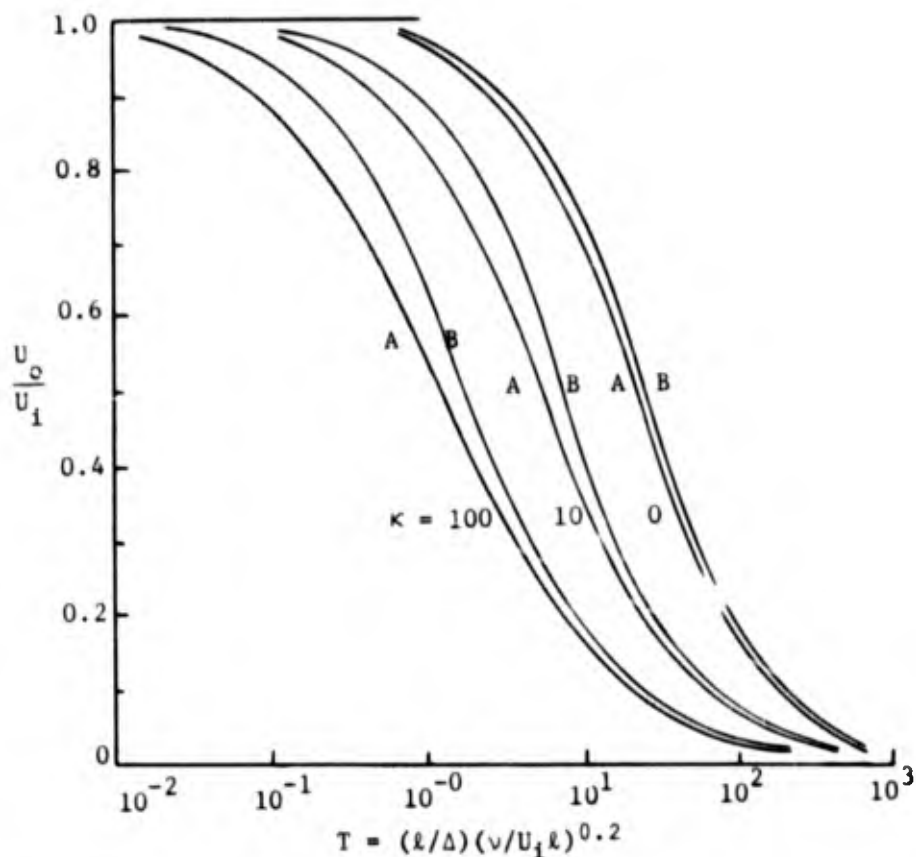
35

Fig. B-6 Recovery factor U_o/U_i as a function of geometry and Reynolds number, for various values of particle loading. The results of the integral method of section 4 are denoted by B and the analytical approximation of Eq (54) by A.

equivalent to moving along a line T = constant. With κ increasing the value of the recovery factor decreases. Very dramatic reduction in the recovery factor is possible by loading the boundary layer with particles to, as little as, $\kappa = 20$, if T is of the order of 10. This figure also shows that increasing the jet injection velocity in the case of high particle loading is not a very efficient way of improving the recovery factor. (This is because the factor T depends on U_i only to the 1/5th power). On the other hand, by the same argument, using a bigger slit would be more efficient.

5. SIMPLIFIED METHOD EXTENDED TO INCLUDE PARTICLES AND BLOWING

The simple method of Section 3 for the case of turbulent boundary layer without any particles ($\kappa = 0$) can be easily extended to the case with particles provided some reasonable assumption for τ_w is made. In order to be consistent with taking U_m constant at its geometrical mean value, we will assume that

$$\tau_w = \frac{C_f}{2} \, \rho_o \, \bar{U}_i U_o \tag{B.49}$$

where $\bar{U}_i$ = effective velocity of the jet, C_f = skin friction coefficient, and $\rho_o = \rho(1 + \kappa)$.

36

Since the heavy particles or droplets will mix very rapidly with the entering wall jet, this mixing should occur with essentially no loss of jet momentum and effective wall jet velocity can be taken as that given prior to Eq (42).

$$\bar{U}_1 = U_o + \frac{U_1 - U_o}{\sqrt{1 + \kappa}} \tag{B.50}$$

If we now use the Blasius flat plate value for C_f

$$C_f = 0.072 \left(\frac{\rho_o U_o \ell}{\mu}\right)^{-0.2} = 0.072 \left(\frac{U_1 \ell}{\nu}\right)^{-0.2} \left(\frac{U_o}{U_1}\right)^{-0.2} (1 + \kappa)^{-0.2} \tag{B.51}$$

Eq (49) becomes

$$\tau_w = 0.036 \left(\frac{U_1 \ell}{\nu}\right)^{-0.2} \left[\frac{U_o}{U_1} (1 + \kappa)\right]^{-0.2} \rho(1 + \kappa) \left[U_o + \frac{U_1 - U_o}{\sqrt{1 + \kappa}}\right] U_o \tag{B.52}$$

Consider this value of τ_w as the average value over the length 'ℓ' and substitute into Eq (17)

$$\rho U_1^2 \Delta = \rho U_1 U_o \Delta + 0.036 \left(\frac{U_1 \ell}{\nu}\right)^{-0.2} \ell\, \rho(1 + \kappa) U_o \left[U_o + \frac{U_1 - U_o}{\sqrt{1 + \kappa}}\right] \left[\frac{U_o}{U_1} (1 + \kappa)\right]^{-0.2} \tag{B.53}$$

$$\left(1 - \frac{U_o}{U_1}\right) = 0.036\, T\, (1 + \kappa)^{0.8} \left(\frac{U_o}{U_1}\right)^{0.8} \left[\frac{U_o}{U_1} + \frac{1}{\sqrt{1 + \kappa}} \left(1 - \frac{U_o}{U_1}\right)\right] \tag{B.54}$$

The recovery factor U_o/U_1 can be obtained as a function of T for various particle loadings. Figure 6 shows the variation of U_o/U_1 with T for $\kappa = 0$, 10 and 100. It can be seen that this simpler method gives a reasonably good estimate of recovery factor (especially for lower values of particle loading (small κ) and higher values of T as compared to the more complicated method of section 4. At high particle loadings and small values of T, there is considerable disagreement between the two methods. This car be attributed to the fact that the relation Eq (49) is not strictly valid in this range, although the accuracy of section 4 itself cannot be determined quite well until it is compared with a more accurate solution.

The model of this section can also be extended quite easily to the case with radial injection at the wall. The effect of radial injection enters directly into the momentum balance and indirectly by its influence on the skin friction at the wall. The influence of uniform radial injection on skin friction in the turbulent boundary layer over a flat plate has been the subject of several investigations[B.6] but for our purposes we can use a simple relation for the modified skin friction which is valid for small blowing and large Reynolds numbers

$$C_f]_{blowing} = [C_{f_o}]\left(1 - \frac{B_o}{2}\right) \qquad (B_o \ll 1) \tag{B.55}$$

where $B_o = \dfrac{(\rho U)_{injection}}{\rho_o U_o} \cdot \dfrac{2}{C_{f_o}}$

C_{f_o} denotes the value of skin friction without blowing. In the present case

$$B_o = \frac{U_r}{(1 + \kappa)\, U_o} \cdot \frac{2}{C_{f_o}} \qquad (B.56)$$

Substituting this expression for C_f into the momentum balance equation and proceeding as before in the case of no radial injection, we have

$$\frac{U_1}{U_o} = 1 + R + \left[1 + \frac{U_1/U_o - 1}{\sqrt{1 + \kappa}} \right] \left[0.036\ T \left(\frac{1 + \kappa}{U_1 U_o}\right)^{0.8} - \frac{R}{2} \right] \qquad (B.57)$$

$$\text{where } R = \frac{\ell U_r}{\Delta U_1} = \dot{m}_r / \dot{m}_1$$

The value of recovery factor is plotted in Fig. (B-7) ($\kappa = 0$) and Fig. (B-8) ($\kappa = 100$) against T for various values of R. At low values of T, increase in blowing tends to decrease the recovery factor whereas at high values, it has an opposite effect. Equation (57) may be rearranged to give Eq (18) in section 5 of the main report.

6. SUMMARY

In this investigation a study of two-phase turbulent boundary layer flow in a vortex has been carried out. On using certain simplifying assumptions each of which has been tested and justified in certain ways, the dependence of the recovery factor on particle loading was calculated. We believe that our result is sufficiently accurate for engineering purposes even though the model used in our analysis is not very elaborate.

This work is by no means complete. Many effects which could be significant under special circumstances e.g. the effect of centrifugal force on the particles have not been taken into account. It is hoped that they will be considered in future studies.

Fig. B-7 Recovery factor U_o/U_i as a function of parameter T, for various values of injection $R(=\dot{m}_r/\dot{m}_i)$ with particle loading $\kappa = 0$, using Eq (57).
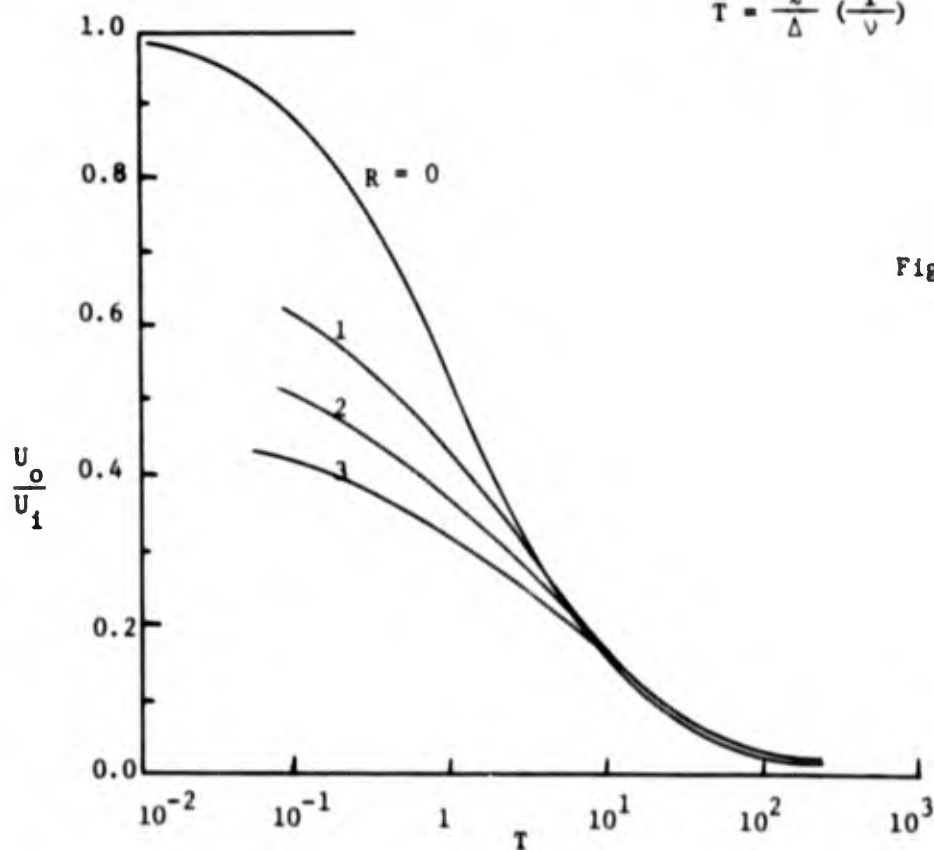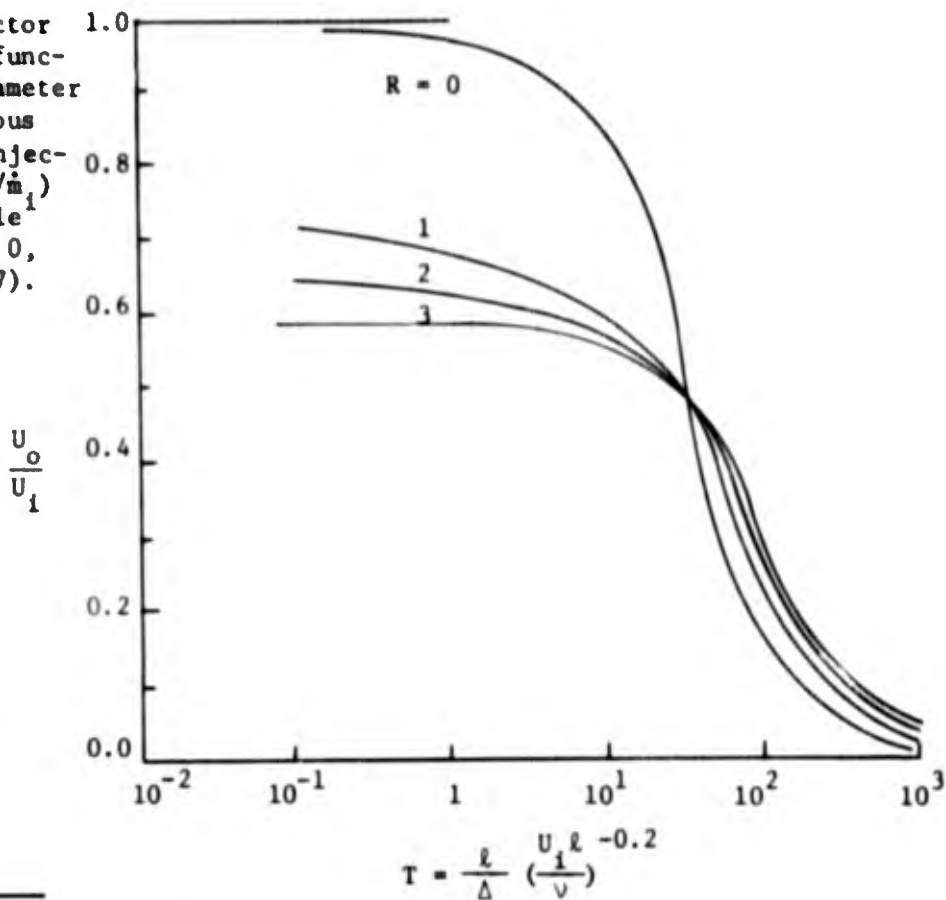

$$T = \frac{\ell}{\Delta}\left(\frac{U_i \ell}{\nu}\right)^{-0.2}$$

Fig. B-8 Recovery factor U_o/U_i as a function of parameter T, for various values of injection $R(=\dot{m}_r/\dot{m}_i)$ with partical loading $\kappa = 100$, Eq (57).

39

REFERENCES

B.1   Keyes, J. J., Jr., Chang, T. S. and Sartory, W. K., <u>Hydromagnetic Stabilization of Jet Driven Vortex Flow</u>, Oak Ridge National Laboratory Report TM-1896, 1967.

B.2   Rodoni, C. A., <u>An Investigation of the Flow Parameters of a Confined Turbulent Vortex</u>, S.M. Thesis, Department of Aero. & Astro., MIT, August 1969.

B.3   Lewellen, W. S., <u>A Review on Confined Vortex Flows</u>, NASA CR-1772, July.

B.4   Roschke, E. J., <u>Experimental Investigation of a Confined Jet Driven Water Vortex</u>, JPL Report 32-982, NASA CR-78550 and <u>Flow Visualization Studies of a Confined Jet-Driven Water Vortex</u>, JPL Report 32-1004, 1966.

B.5   Felsing, G. W., Mockenhaupt, J. D. and Lewellen, W. S., <u>Investigation of a Vortex Value to Control Chamber Pressure in the NERVA Engine</u>, AIAA Paper No. 70-658, 1970.

B.6   Schlichting, H., <u>Boundary Layer Theory</u>, McGraw Hill Co., New York, 1968.